

CONTENTS

Proceedings of the 13th NICT TDC Symposium (Kashima, June 4, 2014)	
Flux monitoring observations of Sgr A* at S and X bands with the NICT VLBI System II 1
<i>Shunya Takekawa, Tomoharu Oka, and Mamoru Sekido</i>	
A New Verification Method of Applied Calibrations onto Visibility Data 3
<i>Makoto Miyoshi</i>	
Report of VLBI Experiments between Australia and Japan 6
<i>Yoshiaki Hagiwara, Syunsaku Suzuki, Tomoaki Oyama, and Takashi Nishikawa</i>	
Receiving performance of Ishioka VGOS Antenna 8
<i>Yoshihiro Fukuzaki, Kojin Wada, Jiro Kuroda, Shinobu Kurihara, Ryoji Kawabata, and Takahiro Wakasugi</i>	
Regular Geodetic VLBI Observation with a Wide-band Recording System 11
<i>Takahiro Wakasugi and Ryoji Kawabata</i>	
The Tian Ma 65-m radio telescope of Shanghai Observatory 14
<i>N. Kawaguchi</i>	
Status of Broadband VLBI Observation System (Gala-V) Development 17
<i>Mamoru Sekido, K. Takefuji, H. Ujihara, M. Tsutsumi, S. Hasegawa, Y. Miyauchi, E. Kawai, R. Ichikawa, Y. Koyama, and T. Kondo</i>	
Development of digital filters toward GHz-width VLBI 20
<i>Kazuhiro Takefuji, Mamoru Sekido, Hideki Ujihara, Masanori Tsutsumi, Shingo Hasegawa, and Tetsuro Kondo</i>	
On a Wide-Band Bandwidth Synthesis 23
<i>Tetsuro Kondo and Kazuhiro Takefuji</i>	
Development of Wideband Feed 28
<i>Hideki Ujihara, Kazuhiro Takefuji, and Mamoru Sekido</i>	
- News - News - News - News -	
The 13th IVS NICT- Technology Development Center Symposium 32

Flux monitoring observations of Sgr A* at S and X bands with the NICT Kashima–Koganei VLBI System II

Shunya Takekawa¹ (*shunya@z2.keio.jp*),
Tomoharu Oka^{1,2}, Mamoru Sekido³

¹ *School of Fundamental Science and Technology, Graduate School of Science and Technology, Keio University*

3-14-1 Hiyoshi, Kohoku-ku, Yokohama, Kanagawa, Japan

² *Department of Physics, Faculty of Science and Technology, Keio University*

3-14-1 Hiyoshi, Kohoku-ku, Yokohama, Kanagawa, Japan

³ *Space-Time Standards Laboratory, Kashima Space Technology Center, National Institute of Information and Communications Technology*
893-1 Hirai, Kashima, Ibaraki, Japan

Abstract: A compact radio source Sgr A* is the nucleus of our Galaxy and harboring a supermassive black hole with the mass of $4 \times 10^6 M_\odot$. While the current activity of the Galactic nucleus is extremely low, an activation subsequent to the infall of the G2 cloud is expected within several years. In order to search for the flux variation which is caused by the interaction between the G2 cloud and the accretion disk, we have been conducting flux monitoring observations of Sgr A* at S band (2 GHz) and X band (8 GHz) using the NICT Kashima–Koganei VLBI system (109 km baseline) since mid-February 2013. Until 3 June 2014, we observed Sgr A* for 42 days. Four quasars (NRAO 530, PKS 1622–253, PKS 1622–297, PKS 1921–293) were also observed as flux calibrators. No significant change nor variation has been detected in the 8 GHz flux density of Sgr A* so far. The 8 GHz flux density was 0.81 ± 0.06 Jy, while no significant 2 GHz emission was detected by our system.

1. Introduction

Milky Way has a $4 \times 10^6 M_\odot$ supermassive black hole (SMBH) at its center, which is recognized as a compact radio source Sgr A*. Despite the huge mass, Sgr A* is extremely dim and quiet. This extreme dimness suggests a very low mass accretion rate ($< 10^{-5} M_\odot \text{ yr}^{-1}$), and/or a low radiation efficiency. On the other hand, the widespread (~ 200 pc) distribution of Fe 6.4 keV fluorescent line emission implies that Sgr A* was far brighter ($\sim 10^{39}$ erg s^{-1}) than the present about several hundred

years ago^[1]. It is possible that currently inactive Sgr A* may be active sometime. Such variations may be caused by intermittent accretion of interstellar gas onto the central SMBH.

Recently, the Max-Planck-Institut für extraterrestrische Physik (MPE) group has reported the discovery of a dense gas cloud, G2, which is on its way toward Sgr A*^[2]. The G2 cloud has the mass of $\sim 3M_\oplus$ and is on the elliptical orbit with high eccentricity. The G2 cloud has been stretched and will be disrupted by the strong tidal force from the central SMBH. The tidal disruption of the G2 cloud will increase mass accretion rate onto the central SMBH, causing a multi-wavelength flare. The interaction between hot plasma around Sgr A* and the G2 cloud may cause a bow shock, accelerating electrons, which emit synchrotron radiation in centimeter wavelength^[3]. The G2 cloud had been expected to reach the pericenter, ~ 2400 Schwarzschild radii from the nucleus, in Spring 2014^{[4][5]}. However, according to the most recent report, the G2 cloud has not yet reached its pericenter^[6].

2. Observations

In order to search for the centimeter-wave flux variations caused by the G2 event, we have conducted flux monitoring observations of Sgr A* at 2 GHz and 8 GHz using the NICT Kashima–Koganei VLBI system since mid-February 2013^[7]. This VLBI system consists of K5/VSSP32 samplers and two 11-m diameter antennas which are located at Kashima and Koganei in Japan. The baseline length is 109.1 km. The observing frequencies are 2.21–2.29 GHz and 8.2–8.5 GHz. The spatial resolutions of this VLBI system are $\simeq 250$ mas and $\simeq 70$ mas at 2 GHz and 8 GHz, respectively. Until 3 June 2014, we observed Sgr A* for 42 days in total, about five hours ($EL > 15^\circ$) each day. Since 78th day-of-year (DOY) 2013, four quasars (NRAO 530, PKS 1622–253, PKS 1622–297, PKS 1921–293) are observed as flux calibrators, while only NRAO 530 had been used before 78th DOY. The integration times are, 300 s, 30 s, 240 s, 240 s, and 30 s, for Sgr A*, NRAO 530, PKS 1622–253, PKS 1622–297 and PKS 1921–293, respectively, in each observing sequence. All the sources were observed by turns in the observing five hours.

3. Results

Figure 1 shows a plot of the 8 GHz flux densities of Sgr A* and the calibrators. No significant emission at 2 GHz has been detected so far. We determined Sgr A* flux by using the correlation amplitudes of calibrators, and the 8 GHz flux of NRAO 530 (5.4 Jy ^[8]). Note that quasars are variable

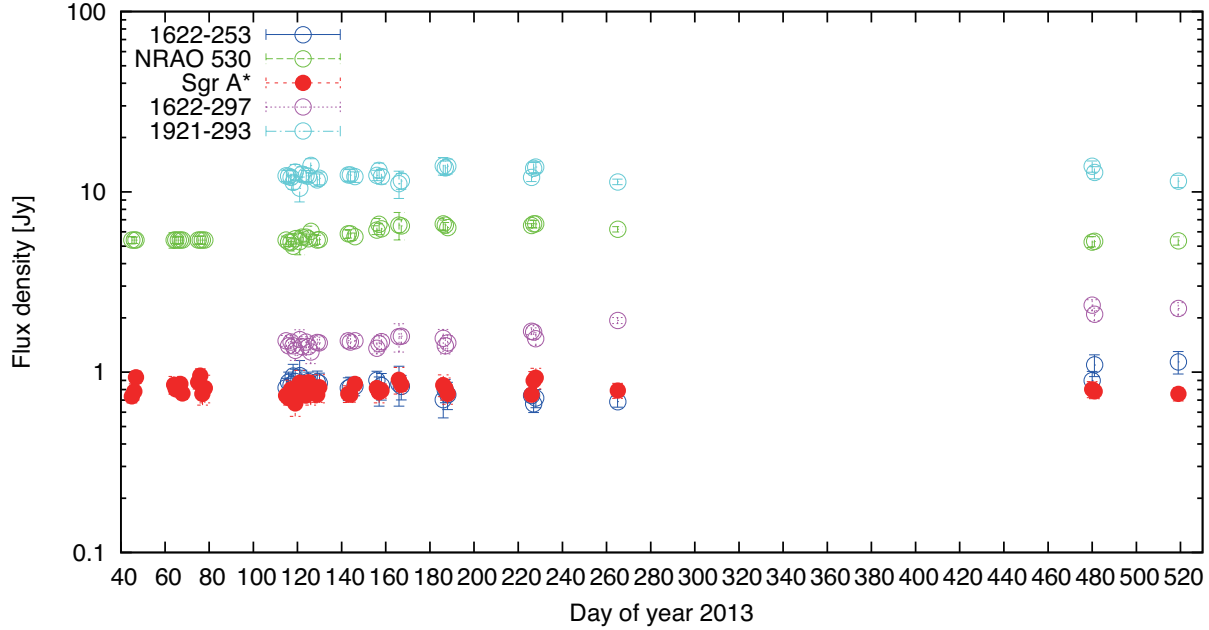


Figure 1. Flux densities of the observed sources at 8 GHz. These flux densities are values averaged over each observing day. Error bars show 1σ standard deviation for each day.

objects in every wavelength, thus the flux calibration method employed here is a little controversial. Nevertheless, the 8 GHz flux of Sgr A* is really stable, exhibiting no significant flare or variation. We obtained the average flux is 0.81 ± 0.06 Jy.

4. Summary

In order to search for the radio flux variations of Sgr A* associated with the G2 event, we have conducted the flux monitoring observations at 2 GHz and 8 GHz with the NICT Kashima-Koganei VLBI system. We obtained the 8 GHz flux densities of Sgr A* from the mid-February 2013 to 3 June 2014 for 42 days, while no significant emission from Sgr A* at 2 GHz has been detected by our system. Sgr A* is very stable at 8 GHz, and the average flux is 0.81 ± 0.06 Jy. These monitoring observations are very important for studies of SMBHs and active galactic nuclei. When the flare is detected in our

monitorings, we will alert it to the world as soon as possible. We intend to continue these monitorings as often as possible for the next several years.

References

- [1] Ryu, S. G., et al. 2013, PASJ, 65, 33
- [2] Gillessen, S., et al. 2012, Nature, 481, 51
- [3] Narayan, R. et al. 2012, ApJL, 757, L20
- [4] Gillessen, S., et al. 2013, ApJ, 774, 44
- [5] Phifer, K. et al. 2013, ApJ, 773, 13
- [6] Eckart, A. et al. 2014, ATEL #6285
- [7] Takekawa, S. et al. 2013, IVS NICT-TDC News, No.33, 18
- [8] Healey, S. E. et al., 2007, ApJS, 171, 61

A New Verification Method of Applied Calibrations onto Visibility Data

Makoto Miyoshi (*makoto.miyoshi@nao.ac.jp*),

National Astronomical Observatory Japan,
2-21-1 Osawa, Mitaka Tokyo, Japan 181-8588

Abstract: Visibility calibrations are essentially important for VLBI astronomical imagings. In general, however, the VLBI data calibrations lack their verification methods testifying the validation. For that reason, too much nervous data flagging often fails to utilize an original spatial resolution of VLBI. Or adversely, incorrect results from improper calibration and analysis can be reported. Therefore, it is better to establish an objective index to show the validity of VLBI data calibrations. We here show our approach to establish such a verification method by comparing statistical property of calibrated visibility data and theoretical prediction from thermal noise property. We have no way of knowing about the structure of observed astronomical source in advance, while thermal noises which will be included in calibrated visibility data can be estimated from measurements of T_{sys} and antenna performance during observations. If we can subtract the components of observed source structure from calibrated visibility data, the residuals of the calibrated visibility should show a statistical property as of pure thermal noise (if the calibrations are correctly performed). If not, the performed calibrations are not sufficient for reducing systematic errors from visibility data and the resultant synthesis images should be not perfectly correct. Here we show such a trial using calibrated visibility data of Miyoshi et al. (2011)[1] and demonstrate their visibility data calibrations are correctly performed.

1. Statistical Behavior of Visibility

Statistical behavior of visibility including signal and thermal noise is theoretically well known. Below we show the equations modified from Thompson et al. (2001)[2] but the definition is modified suitable for the issue. The measured (**and correctly calibrated**) visibility is represented by a vector $Z = V + \epsilon$ where V and ϵ represent the true visibility (the signal) and noise components, respectively. Because the observed source has a complex structure in general the signal V is presented as a vector so that $V = (V_x, V_y)$. The phase of the measured visibility is here denoted by ϕ . The components of ϵ have independent zero-mean

Gaussian probability distributions in the x and y coordinates with an rms deviation σ given by Eq. (6.43) in Thompson et al. (2001)[2]. Z have a probability distribution given by

$$p(Z_x, Z_y) = \frac{1}{2\pi\sigma^2} \exp\left(-\frac{(Z_x - V_x)^2 + (Z_y - V_y)^2}{2\sigma^2}\right) \quad (1)$$

It is often useful to deal with the magnitude and phase of the visibility, denoted by Z and ϕ . Respective probability distributions are:

$$p(Z) = \frac{Z}{\sigma^2} \exp\left(-\frac{Z^2 + |V|^2}{2\sigma^2}\right) I_0\left(\frac{Z|V|}{\sigma^2}\right) \quad (2)$$

where $Z = \sqrt{Z_x^2 + Z_y^2}$.

$$p(\phi') = \frac{1}{2\pi} \exp\left(-\frac{|V|^2}{2\sigma^2}\right) \left\{ 1 + \sqrt{\frac{\pi}{2}} \frac{|V| \cos \phi}{\sigma} \cdot \exp\left(\frac{|V|^2 \cos^2 \phi'}{2\sigma^2}\right) \times [1 + \text{erf}\left(\frac{|V| \cos \phi'}{\sqrt{2}\sigma}\right)] \right\} \quad (3)$$

where I_0 is the modified Bessel function of order zero, and erf is the error function. ϕ' is the phase angle measured from the direction of V vector.

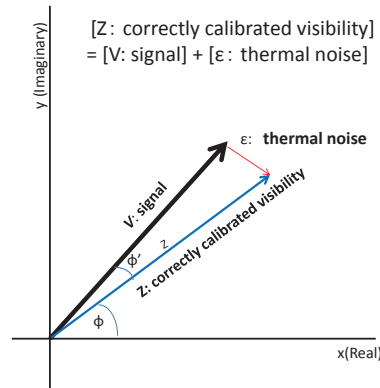


Figure 1. Definition of Visibility

2. Difference of Visibilities between Channels

Because the source structure is unknown to us in general, we cannot predict how the signal V behave. If we can subtract the V from the visibility Z , the residual is a pure noise ϵ , whose nature can be estimated from measured system temperatures

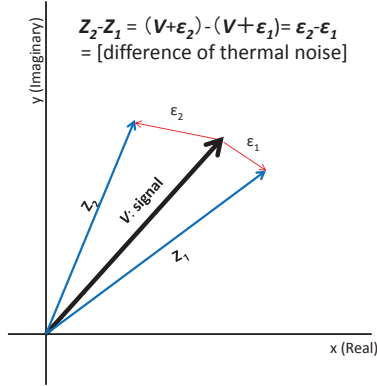


Figure 2. Cancellation of Signal in Visibility

and antenna performance. A difference of visibilities between different video channels recorded at the same time with the same baseline corresponds to such quantities. If the applied calibrations to the visibilities are precisely appropriate, the difference should statistically show the noise nature. As for the distribution function of amplitude difference of visibilities, we found the following formula. We denote the amplitude difference of visibilities as t which can be negative.

$$\begin{aligned}
 p(t) = & + \frac{\sqrt{\pi}t \exp(-\frac{t^2}{4\sigma^2}) \operatorname{erf}(\frac{|t|}{2\sigma})}{8\sigma^3} \\
 & - \frac{\sqrt{\pi}t \exp(-\frac{t^2}{4\sigma^2}) \operatorname{erf}(\frac{|t|}{2\sigma})}{4\sigma|t|} \\
 & - \frac{\sqrt{\pi}t^2 \exp(-\frac{t^2}{4\sigma^2})}{8\sigma^3} \\
 & + \frac{\sqrt{\pi} \exp(-\frac{t^2}{4\sigma^2})}{4\sigma} \\
 & + \frac{t \exp(-\frac{t^2}{2\sigma^2})}{4\sigma^2} \quad (4)
 \end{aligned}$$

As for the distribution function of phase difference of visibilities, we found that the function has no analysis solution, however, we can make a concrete table from numerical solution.¹ Here we assumed the same noise level in respective channel.

3. Real Distribution of Visibility Difference

By checking the distributions of difference of visibilities of recording channels, we can verify the ap-

¹The equation shown in Miyoshi et al. (2011)[1] is incorrect.

plied calibrations are proper or not. If the distributions followed those of difference between thermal noises, the calibrations are proper and the resultant synthesis images are free from systematic errors. In Figure 3, we show examples of real distributions of visibility difference both in amplitude and phase from calibrated visibility data in Miyoshi et al. (2011)[1]. The data were calibrated in each channel individually using tasks like FRING and CALIB in AIPS, the obtained solutions for delay, rate, phase and amplitude are totally independent for each channel. Both of distributions are fitted the theoretical thermal noise curves quite well so that the applied calibration solutions to the visibility data reduced systematic errors properly. We checked not only these but all of differences between all channels in all base lines except MK-baselines and found that 92.56% of amplitude differences and 87.20% of phase differences are within 95% confidence level of Chi-square test. Which means almost of data set were well calibrated by their manner. We further made synthesis images using visibility data set within $3 - \sigma$ distributions and the resultant images are almost the same as ones reported in Miyoshi et al. (2011) [1]. These results demonstrated that their report of QPO detections in SgrA* from VLBA images were not caused from systematic errors by improper calibrations.

4. Summary

By checking distributions of differences of visibility (both in amplitude and in phase) between recording channels obtained from the same baseline at the same time, we can testify the validation of the applied calibrations to the data. Using this method we proved that the image-QPO detection in Miyoshi et al. (2011) [1] are not from improper calibrations of VLBA data. About the details we will report in our preparing paper.

5. Acknowledgments

We thank Nitta S. for his kind analytical calculations for the distributions of difference of visibilities.

References

- [1] Miyoshi, M., Shen, Z-Q., Oyama, T., Takahashi, R., Kato Y., *Publ. Astron. Soc. Japan*, **63**, p1093-1116 (2011).
- [2] Thompson, A. R., Moran, J. M., Swenson, G. W., (2001), *Interferometry and synthesis in radio astronomy*, 2nd ed., John Wiley & Sons, Inc.

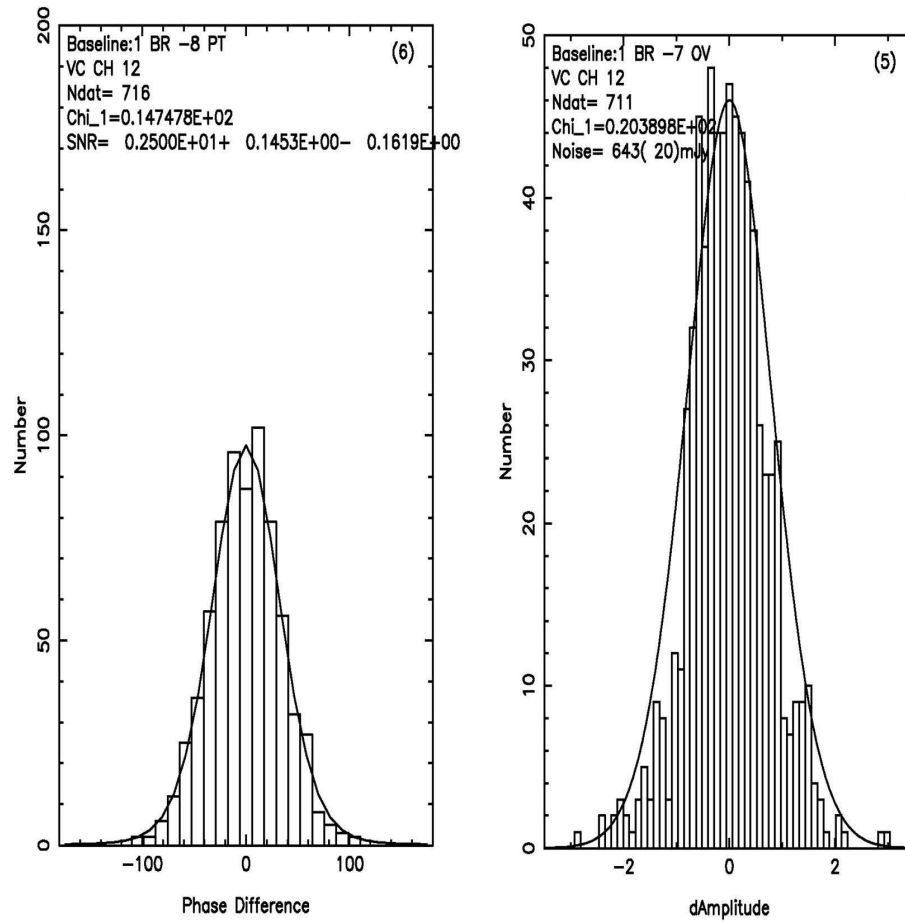


Figure 3. Distributions of Visibility Difference. Those of Phase (left) and Amplitude (right)



Report of VLBI Experiments between Australia and Japan

Yoshiaki Hagiwara

(*yoshiaki.hagiwara@nao.ac.jp*), **Syunsaku**

Suzuki, Tomoaki Oyama, Takashi

Nishikawa, *National Astronomical Observatory of Japan 2-21-1 Osawa, Mitaka, Tokyo 181-8588, Japan*

Shinji Horiuchi(*shoriuchi@cdscc.nasa.gov*)

CSIRO Astronomy and Space Science, Canberra Deep Space Communications Complex, PO Box 1035, Tuggeranong, ACT 2901, Australia

Abstract: We report on recent VLBI experiments linking the DSN-Tidbinbilla 70m telescope in Australia with the four 20m telescopes of VERA in Japan in early 2014. The data recorded at each telescope were shipped to to Mitaka in Japan and processed using the NAOJ software correlator (Softcos), resulting to successful fringe detection. The maximum telescope separation in this experiment was over 8,300 km, and an resultant angular resolution is 0.38 arcsecond at 22 GHz. The ambitious plan for this experiment is to connect the Tidbinbilla 70m to the East Asia VLBI Network (EAVN) across the Pacific Ocean.

1. Introduction

VLBI experiments have been conducted by the radio telescopes in East Asia VLBI Network (EAVN) in which 14 telescopes in China, Japan, and Korea participated. Many attempts to organize the East Asia VLBI Network (EAVN) have been made for radio astronomy observations. The EAVN will combine more than 10 radio telescopes distributed over the countries of China, Japan, and Korea. One of the aims of the EAVN is to obtain a better angular resolution that is provided telescope separation between China and Japan and improved imaging sensitivity by adding large telescopes such as the new 65m telescope in Shanghai. It should be noted that scientific results of astronomy using the EAVN have been reported [1].

The EAVN has a more ambitious plan to extend its maximum telescope separation that is currently limited to at most 5,500 km. In order to extend telescope separation for obtaining a better angular resolution, we organized VLBI experiments by linking the Tidbinbilla 70m telescope in Australia with the VERA (VLBI Exploration of Radio Astrometry) in Japan. This might extend outside Asia and Australia.

2. Experiment Conditions

The experiments were conducted on February 23 in 2014 by employing four 20m telescopes of VERA and the Tidbinbilla 70m telescope (DSS-43) located in the Canberra Deep Space Communication Complex (CDSCC). The experiments were conducted at 22 GHz for sources of Orion-KL and 0420-014 and total time of the experiments was about 1 hour. The parameters of the experiments are summarized in Table 1.

VLBI Data were recorded with 1024 Mbps (16 channels x 16 MHz x 2 bits/sample) recording rate at each site using the Mark 5C terminal of the Tidbinbilla 70m and the OCTADISK for VERA. The data obtained at each site were converted to files following the VLBI Data Interchange Format (VDIF) [2]. The data were then transmitted to the correlator center at the National Astronomical Observatory of Japan (NAOJ) in Tokyo via network and processed on the NAOJ soft correlator system (Softcos) after the experiments. A schematic diagram describing the experiments is shown in Fig.1.

Table 1. VLBI experiments

Telescopes	DSN-Tidbinbilla, VERA
Observation date	2014 February 24
Duration	1 hour
Frequency	22.235 GHz
Rec terminals	Mark5C(Tid), OCTADISK(VERA)
Sources	Orion-KL, 0420-014
Data processor	NAOJ Software Correlator

3. Results

Fringes between the 70m and VERA using 8 seconds of data were detected in the both spectral-line (Orion-KL) and continuum (0420-014) sources (Fig.2). For example, the peak of the fringe amplitude of Orion-KL from the Mizusawa-Iriki baseline (~1,200 km) was obtained in signal-to-noise ratio (SNR) of 620, while the fringe from the Iriki-Tidbinbilla baseline (~8,100 km) was detected in SNR of 430. This demonstrates that the source structure of the maser in Orion-KL is more resolved by the longer Australian baseline. The same trend can be seen for the fringe of the continuum source (0420-014): The fringe peak amplitude of the Mizusawa-Iriki baseline was obtained in SNR of 15, while that of the Mizusawa-Tidbinbilla baseline was 10, which shows that the source structure of the quasar, 0420-014 was certainly more resolved by the longer baseline.

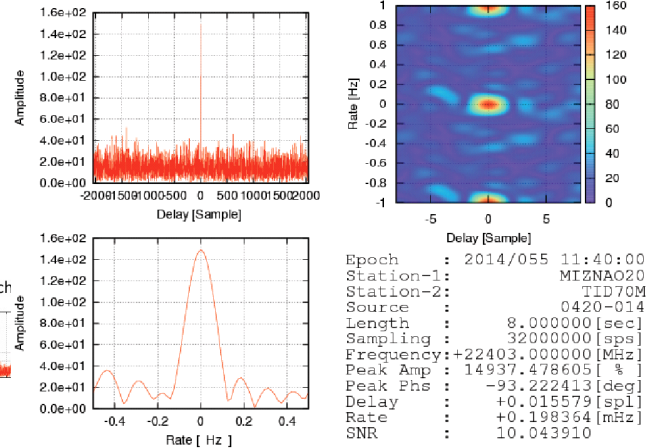
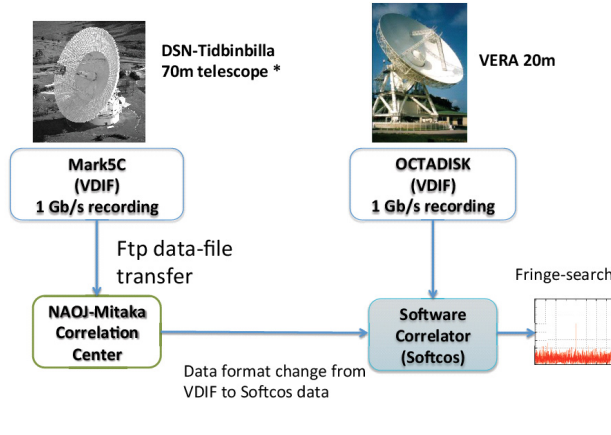


Figure 1. Schematic diagram of the VLBI experiment: The data in VDIF format were recorded with 1 Gbps recording rate at Tidbinbilla and VERA each. After the experiments, data files of the Tidbinbilla were transmitted to the correlator center at NAOJ via network and fringe-search was made by the software correlator (Softcos).

Figure 2. The fringe plot of the Tidbinbilla-Mizusawa (VERA) baseline for the source of 0420-014: Fringe was detected in SNR of 10 using 8 seconds data. The data were processed using the Softcos at NAOJ.

4. Summary

We succeeded in the fringe detection in the VLBI experiments connecting the 70m telescope at Tidbinbilla in Australia with 20m VERA telescopes distributed over Japan. The maximum telescope separation in this experiment was over 8,000 km, resulting in a resolution of 0.38 arc seconds, ~ 1.5 times better than that of the EAVN or ~ 4 times better than the VERA (Table 2). The ambitious plan for this experiment is to connect telescopes in Australia to the EAVN. In future, those telescopes are expected to be connected via the fiber network across the Ocean to transmit data for nearly real-time correlation. This idea might extend to outside Australia and east Asia.

5. Acknowledgments

We are grateful to Dr. Shinji Horiuchi and other staff for support for this experiment at the Tid-

binbilla 70m telescope in the Canberra Deep Space Communication Complex.

References

- [1] Fujisawa, K., Sugiyama, K., Motogi, K., Hachisuka, K., Yonekura, Y., et al., Observations of 6.7 GHz methanol masers with East-Asian VLBI Network. I. VLBI images of the first epoch of observations, Publications of the Astronomical Society of Japan, Vol. 66, Issue 2, 31 (1-29), 2014
- [2] Sekido, M., Takefuji, K., Kimura, M., Hoberger, T., Kokado, K., Nozawa, K., Kurihara, S., Shinno, T., Takahashi, F., Development of an e-VLBI Data Transport Software Suite with VDIF, in Proceedings from the 2010 General Meeting, "VLBI2010: From Vision to Reality", February, 2010 in Hobart, Tasmania, Australia. (eds) D. Behrend and K.D. Baver. NASA/CP 2010-215864., p.410-414, 2010

Table 2. Array performance

Telescope	Diameter [m]	T_{sys} [K]	SEFD [Jy]	B^a [km]	θ^b [arcsec]	σ^c [mJy]
DSN-Tidbinbilla	70	40	48	0	0	-
VERA	20	150	2400	8336	0.38	2.2
(Kashima ^d)	34	140	304	7990	0.41	0.78

a) Baseline length
 b) Angular resolution
 c) One sigma baseline sensitivities, assuming 256 MHz bandwidth and 60 seconds integration time
 d) Estimation by assuming that the NICT Kashima 34m telescope participated to this experiment

Receiving performance of Ishioka VGOS Antenna

Yoshihiro Fukuzaki (*fukuzaki@gsi.go.jp*),
Kojin Wada, Jiro Kuroda, Shinobu
Kurihara, Ryoji Kawabata, Takahiro
Wakasugi

*Geospatial Information Authority of Japan,
Kitasato-1, Tsukuba, Ibaraki, Japan*

Abstract: The Geospatial Information Authority of Japan (GSI) has started a new project for constructing a VGOS station in Japan. The construction of the antenna (radio telescope) has been complete and the necessary equipments (Front-end, Back-end, H-maser, and so on) have also been delivered. The name of the new site is Ishioka, which is located 17 km away from Tsukuba 32-m antenna.

We briefly report the current status of the construction of the new antenna, and the initial receiving performance of the antenna and front-end system.

1. Introduction

The Geospatial Information Authority of Japan (GSI) has carried out VLBI observations since 1981. In the first period from 1981 to 1994, we developed transportable VLBI systems with a 5-m antenna and a 2.4-m antenna, and carried out domestic observations by using them. As a result, 8 sites in Japan were observed and precise positions determined. In addition, Japan-Korea VLBI observations were carried out by using a transportable 3.8-m antenna in 1995. In these observations, the Kashima 26-m antenna, which was removed in 2002, was used as a main station. Next, in the second period from 1994 to 1998, GSI established four permanent stations: Tsukuba 32-m, Sintotsukawa 3.8-m, Chichijima 10-m and Aira 10-m antennas. Up to the present, regular VLBI observations by using the four stations have been carried out. Especially, Tsukuba 32-m antenna is a main station for not only domestic but also international VLBI observations now.

In 2011, GSI started a project for constructing a new antenna following the VLBI2010 concept, which is recommended by the International VLBI Service for Geodesy and Astrometry (IVS) as the next-generation VLBI system.

This paper gives the outline of the project, the current status of the construction of the new antenna, and the receiving performance of the antenna and front-end system as the initial result of the performance measurement.

2. Observing Facilities

In the new project, observing facilities are now being constructed. The conceptual design consisting of the six components is depicted in Figure 1. The temporary operations rooms are installed instead of the Operations Building, which will be complete by the end of 2015.

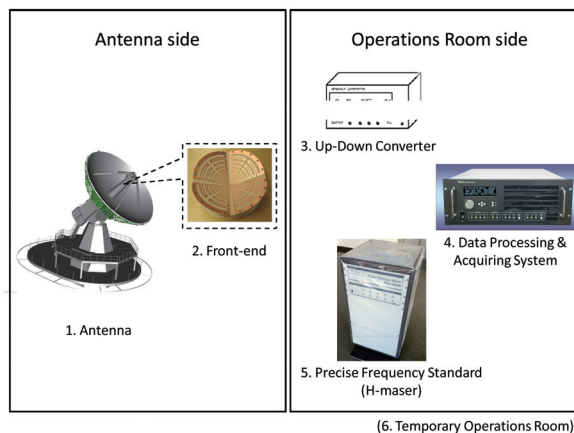


Figure 1. Conceptual design of the new observing facilities

3. Receiving Performance

3.1 Antenna

The antenna (radio telescope) is the main part of the observing system (Figure 2). Since a single antenna is employed, very high slew rates are specified in order to be compliant with the VLBI2010 concept. In addition, Ring Focus optics is applied for the antenna design in order to match the beam pattern of the broadband feed. The receiving performance of the antenna with tri-band feed system was measured by receiving some strong radio stars (Cas-A, Taurus-A, Virgo-A). As a result, the SEFDs for S and X band are approximately 1,700Jy and 1,300Jy, respectively. This means that the aperture efficiencies for S and X band are 59% and 77%, respectively, if the system noise temperature is assumed as 50K. High receiving performance for X band is confirmed as the feature of the Ring Focus optics.

On the other hand, RFI is more serious than expected because of the feature of Ring Focus optics. In the case of Ring Focus optics, the aperture efficiency is better but the artificial radio signal can be reach the feed more easily than the usually-used optics like Cassegrain. In the new station, the radio signal for cellular phone is so strong in the frequency range less than 2.1GHz that the saturation of the amplifier for S band may occur. Installation

of the High Pass Filter to cut the frequency less than 2.2GHz is necessary to avoid the saturation of the S band amplifiers. The specifications and the performance of the antenna are listed in Table 1.



Figure 2. Photo of the new antenna.

Table 1. Specifications and performance of the new antenna.

Parameter	Value
Diameter	13.2 m
RF frequency range	2–14 GHz
Optics	Ring Focus
Surface accuracy	≤ 0.1 mm (rms)
Measured SEFD	1,700Jy (S band) 1,300Jy (X band)
Measured Aperture efficiency	59% (S band) 77% (X band)
AZ maximum slew rate	12°/sec
EL maximum slew rate	6°/sec
AZ maximum acceleration rate	3°/sec ²
EL maximum acceleration rate	3°/sec ²
Special feature	Reference point can be measured directly from the ground for collocation.

3.2 Front-end

According to the VLBI2010 concept, a broadband feed is necessary to achieve high aperture efficiency over 2–14 GHz. At present the Eleven feed, which has been developed at Chalmers University

of Technology in Sweden, and Quadruple-Ridged Flared Horn (QRFH), which is developed at California Institute of Technology (Caltech), are the practical as a broadband feed, so both feed systems are purchased. The employment of the feed will be determined after the evaluation of the antenna performance with these two feeds. For the design of the antenna optics, employing the Eleven feed was assumed.

In the both cases, the feeds and Low Noise Amplifiers (LNAs) are integrated into the each cryogenic system, whose physical temperature is less than 20K. The measured receiver noise temperatures for QRFH system are less than approximately 30K for the both polarizations (see Figure 3.). In addition, in order to achieve the compatibility with the legacy S/X band observation, tri-band feed system is also purchased, and used for the measurement of the initial receiving performance. (See the above section)

The phase and cable calibration system are also installed. A new type of P-cal unit is developed and employed. In addition, instead of the present D-cal a new cable calibration system developed by NICT is also employed. The specifications of the front-end are shown in Table 2.

Table 2. Specifications of the front-end.

Parameter	Value
RF frequency range	2–14 GHz
Polarization	Dual linear polarization
Feed	Eleven feed or QRFH
Dewar	Feed, LNAs, and other devices should be included and cooled by cryogenic system.
Physical temperature	≤ 20 K
Receiver noise temperature	≤ 30 K
Total gain	≥ 45 dB
Output frequency range	2–14 GHz
Number of output	2 (for dual linear polarization)
Phase and delay calibration	New-type P-cal unit New cable calibration system developed by NICT
Injection of P-cal/noise-source	In the front of the feed (Eleven feed) or the front of LNA (QRFH)

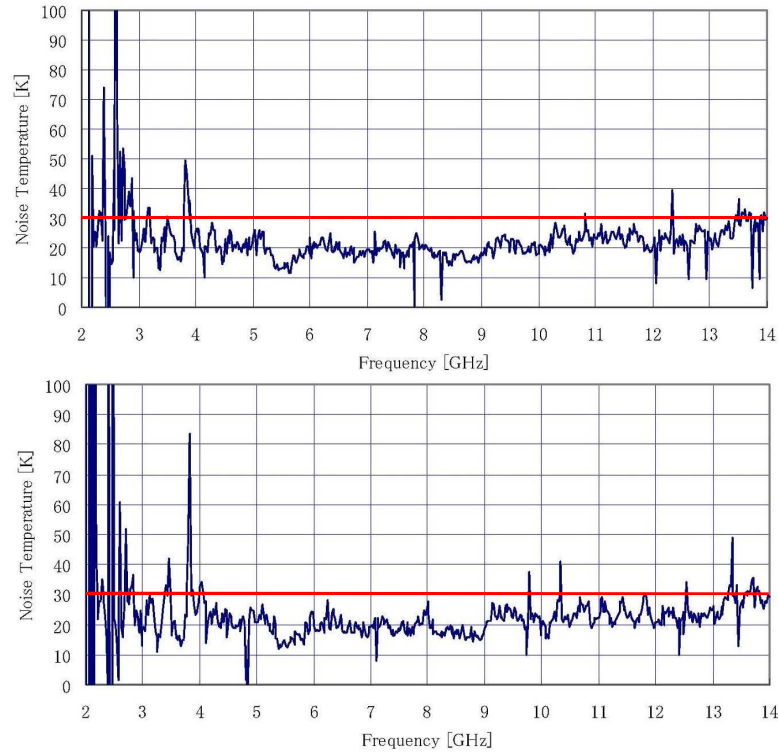


Figure 3. Receiver noise temperature for QRFH system (Upper: Horizontal polarization, Lower: Vertical polarization.)

4. Site Information

The site name is Ishioka, which is near Tsukuba (about 17km-NE from GSI). The location is shown in Figure 4. According to the results of a soil investigation of the site, the bedrock is located near to the surface at less than 3 meter depth, which could avoid the groundwater effects in contrast to Tsukuba 32-m station.

5. Summary

A new project for constructing a new antenna in Japan has started. The new station will be fully compliant with the VLBI2010 concept. The construction of the antenna was complete by the end of March 2014. The measurement of the receiving performance of the antenna was done, and high aperture efficiency for X band is confirmed. Implementation of the station will be done continuously to start regular VLBI observation from April, 2015, and this station will play an important role as a main station in the Asian region in the future.

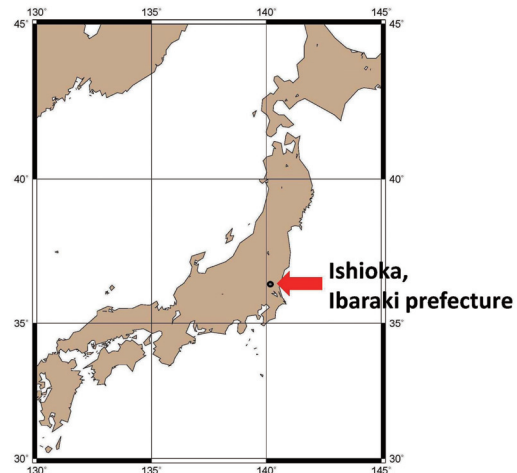


Figure 4. Location of the site of the new observing facilities.

Regular Geodetic VLBI Observation with a Wide-band Recording System

Takahiro Wakasugi (*t-wakasugi@gsi.go.jp*),
Ryoji Kawabata

*Geospatial Information Authority of Japan,
Kitasato-1, Tsukuba, Ibaraki, Japan*

Abstract: Aira VLBI Station, which is one of the VLBI stations operated by the Geospatial Information Authority of Japan (GSI), had taken part in IVS-R1 sessions while Tsukuba VLBI Station could not participate in all IVS sessions due to damage to the substructure of the antenna during 2013. For this purpose, we installed a wide-band recording system. After the improvement of the initial instability of the system, we succeeded in obtaining good data and showed the usefulness of the system for regular VLBI experiments.

1. Introduction

The Geospatial Information Authority of Japan (GSI) has participated in a lot of international VLBI sessions under the framework of International VLBI Service for Geodesy & Astrometry (IVS) in order to maintain the International Terrestrial Reference Frame and to observe the Earth Orientation Parameters. GSI has also carried out domestic (JADE) sessions to determine the position of Japanese land on ITRF and to monitor plate motions around Japan by using four domestic radio telescopes (Figure 1).

Tsukuba VLBI Station is not only main facility of GSI but also one of the central stations in eastern Asia. It has regularly taken part in IVS-R1, IVS-INT2, IVS-INT3, IVS-T2 and JADE sessions. However, Tsukuba had suspended all the sessions from early May to the end of November 2013 due to damage to the substructure of the antenna[1]. Instead of Tsukuba, we decided to take part in IVS-R1 sessions with Aira VLBI Station (Figure 2), which had mainly participated in IVS-T2 and JADE so far. The specifications of the Aira VLBI Station are summarized in Table 1.

2. Recording System

Before participating IVS-R1 sessions, we had to modify the recording system of Aira because the ordinary recording system, which is usually used for JADE, could not record the frequency sequences of IVS-R1 sessions. Especially, the video converter had a selection of 2MHz or 4MHz bandwidth for

one channel, but it was necessary to select 8MHz in order to participate in IVS-R1 sessions. In addition, we also modified down converter a little to be adaptable for IVS-R1 frequency sequences.

In order to record the frequency sequence of IVS-R1 sessions, we employed high speed A/D sampler ADS3000+ and the versatile data recording system K5/VSI (Figure 3) instead of K5/VSSP recording system with the video converter. ADS3000+ is a high speed A/D sampler, which is developed by NICT, JAXA/ISAS and COSMO RESEARCH Corp[2]. ADS3000+ can sample analog data 1Gbps*4ch and output digitized signal 64Msps*16ch for maximum by Digital Base-Band Converter (DBBC) with VLBI Data Interchange Format (VDIF). K5/VSI is a data recording and transferring system, which is also developed by NICT[3]. K5/VSI system is configured by a commercial Linux PC with PC-VSI board and RAID controller board that are both inserted into the expansion bus slot. It can record data with up to 2Gbps at the maximum recording speed. The data sampling and recording process with a set of digital back-ends are adaptable for the coming new VGOS observations.

The sampled data by ADS3000+ were recoded into the RAID 0 system that was configured by some of hard disks with K5/VSSP format by VDIF/SUDP recording control software. The recorded data was converted to mark5b format and simultaneously transferred to the hard disks attached by USB. The hard disks were shipped to Tsukuba soon after finishing sessions. Finally, the data were e-transferred to the correlator from Tsukuba via Internet.



Figure 1. Geodetic VLBI network of GSI.

Table 1. Aira VLBI antenna specifications.

Owner and operating agency	Geospatial Information Authority of Japan
Approximate position	130° 35' 59.51" E, 31° 49' 25.66" N
Year of construction	1997
Radio telescope mount type	Az-El
Antenna optics	Cassegrain
Diameter of main reflector	10 m
Azimuth range	20 – 700°
Elevation range	5 – 88°
Az/El drive velocity	3°/sec
Tsys at zenith (X/S)	120 K / 150 K
SEFD (X/S)	10300 Jy / 7400 Jy
RF range (X1)	8180 – 8680 MHz
RF range (X2)	8580 – 8980 MHz
RF range (S)	2120 – 2520 MHz
Recording terminal	K5/VSSP, ADS3000+ with K5/VSI



Figure 2. Aira VLBI Station.

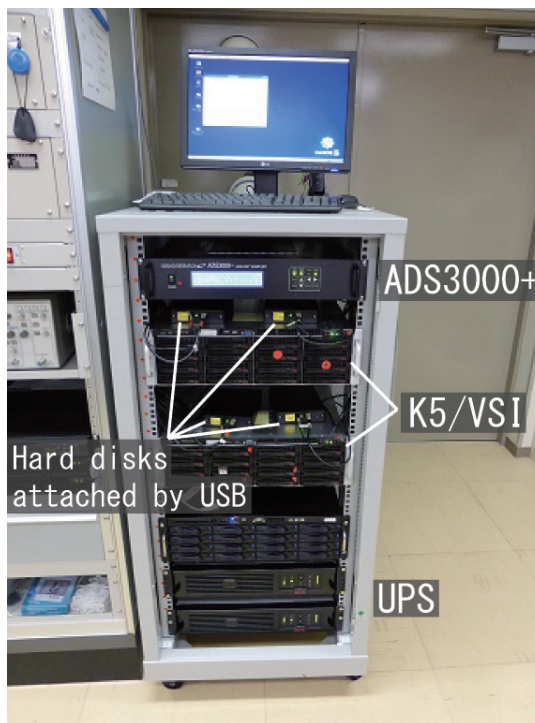


Figure 3. ADS3000+ and K5/VSI recording system in Aira.

3. Result

Aira participated in IVS-R1 sessions 20 times from R1604 (Sep 2013) to R1613 (Nov 2013) and from R1621 (Jan 2014) to R1630 (Mar 2014). However, we missed large number of scans at the initial sessions because of the insufficient memory capacity of the PC that composed K5/VSI recording system. Moreover, the RAID controller board that was also installed in the PC was unstable. We operated multiple K5/VSI system as recording servers and replaced the RAID controller boards with new

ones. Finally, we were able to record most of observations successfully.

The number of the missed scans is shown in Figure 4. The missed scans were drastically decreased by the addition of recording servers and the improvement of the RAID controller board.

Furthermore, the help of NICT with new, more stable recording control software enabled us to perform later sessions certainly. As a result, the missed scans became almost zero from the latter half sessions. The percentage of the correlated

baseline to the scheduled are also shown in Figure 4. The percentage has certainly increased in accordant with the improvement and been kept with high level after that.

4. Summary

We carried out some VLBI experiments of IVS-R1 sessions by using Aira VLBI Station instead of Tsukuba, which faced to serious trouble of the sub-structure. We recorded the observation data with high-speed A/D sampler ADS3000+ with DBBC and K5/VSI data recording system. The improvement of the performance of the PC that composed recording system allowed us to obtain good data stability. We showed that the system was useful for regular VLBI experiments.

Finally, we sincerely thank for the NICT VLBI members who gave us very kindly help.

References

- [1] Wakasugi, T., Status report of the Tsukuba VLBI Station - damage of the antenna base-ment due to over loading -, TDC News, IVS NICT-TDC News, No.33, pp.8-10, 2013.
- [2] Takefuji, K., M. Tsutsumi, H. Takeuchi, Y. Koyama, Current Status of Next Generation A/D Sampler ADS3000+, TDC News, IVS NICT-TDC News, No.31, pp.6-9, 2010.
- [3] Koyama, Y., T. Kondo, M. Sekido, M. Kimura, Developments of the K5/VSI System for Geodetic VLBI Observations, TDC News, IVS NICT-TDC News, No.29, pp.15-18, 2008.

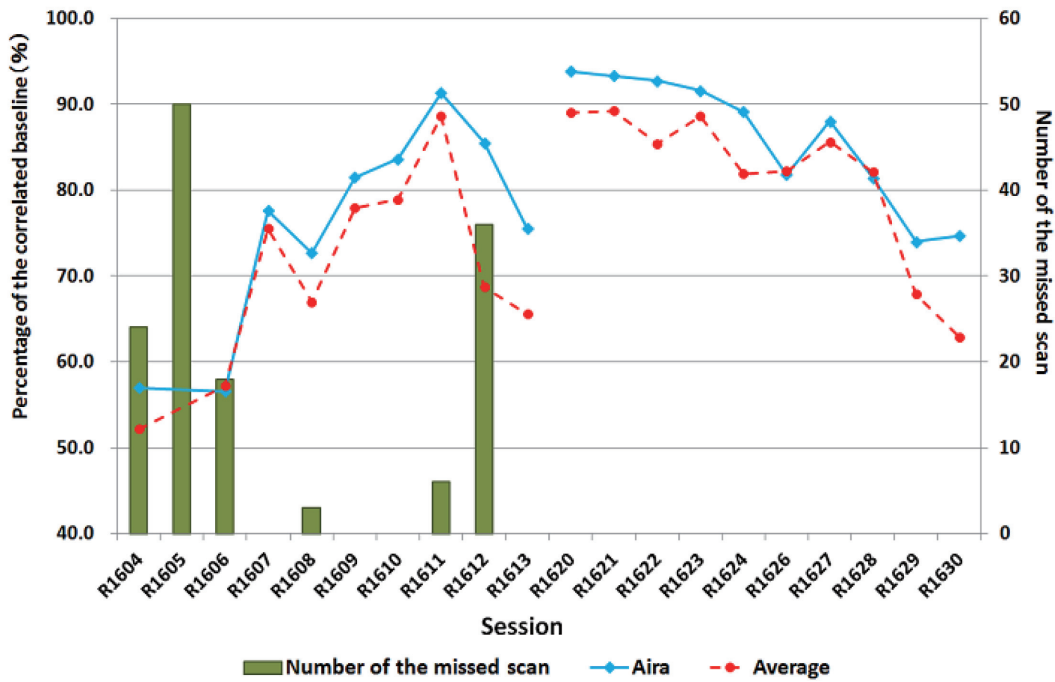


Figure 4. The session status of the Aira VLBI Station. The bar graph shows the number of the missed scan. The percentage of the correlated observations to the scheduled is also described in this plot. The solid line is percentage of Aira, the broken line is that of the average of all stations.

The Tian Ma 65-m radio telescope of Shanghai Observatory

N. Kawaguchi (*kawagu.nori@nao.ac.jp*)

Shanghai Astronomical Observatory

1. Introduction

The Tian Ma 65-m radio telescope (Fig. 1) was constructed in 2012 and was started in the operation in 2013. Now it was primary used in the space project (Chinese moon exploration project, Change) in frequency bands of 2- and 8-GHz. It was operated for radio astronomy observations, Pulsars, Hydrogen and Carbon recombination lines in 1.6-, 2.3- and 5-GHz. The telescope is the largest and the most sensitive radio telescope in the east Asian region, and is expected as a major telescope in the EAVN, East Asian VLBI Network.

In this paper I present the recent activities on developing new facilities to be installed into the 65m telescope. New frequency bands of Ka, K and Q-band are going to be added to the 65-m. In order to keep aperture efficiency in such high frequency bands, it is inevitable to keep the best optimized shape at low and high elevation angles by compensating the unexpected gravitational deformation caused on a large main reflector. In this paper an active surface control system is also presented.

The sheshan campus of the shanghai observatory was established very recently since 2013. So also the brief introduction of the new campus is presented here.



Figure 1. The Tian Ma 65m telescope



Figure 2. The Tian Ma 65m telescope

1.1 Location

The geometry around the Sheshan is shown in fig.2. The 65-m telescope is located at 3-km west to the Sheshan Campus, opposite side of the 25-m telescope. The 25-m telescope was founded almost 25 years ago but still has been working for the international VLBI observation. The 65-m telescope is connected to the 25-m with an optical fiber cable and near-real-time fringe detection is possible on the baseline between the 65-m and the 25-m telescopes. The DiFX correlator is working at the Sheshan Campus.

1.2 Sheshan Campus

The sheshan campus was opened in 2013, where research staffs and students have just started working. In this campus we have a main hall (Fig.3) and research offices (Fig.4). In the main hall computer facilities for VLBI correlation and space data analysis are installed. A big conference room with a large display attached on the all span of the wide wall. In the reserch building offices of the research staffs and students are prepared.



Figure 3. The main hall of the Sheshan Campus



Figure 4. The research building of the Sheshan Campus

2. Toward High Frequency Observation

The 65-m telescope is now working in frequency bands lower than 9GHz, i.e. L-band (1.25-1.75GHz), S-band (2.2-2.4GHz), C-band (4-8GHz) and X-band (8.2-9GHz). New frequency bands, i.e. Ku-band (12-18GHz), K-band (18-26.5GHz), Ka-band (30-34GHz) and Q-band (35-50GHz) are going to be added. In such high frequency bands, however, the gravitational deformation of the main reflector is a serious problem to keep the high efficiency. On the 65-m telescope many actuators are set behind the pannels to compensate the gravitational deformation. Before starting the active surface control, the measurements of the surface accuracy were started.

2.1 Holographic Surface Measurement by a Satellite Signal

To see the potential accuracy of the main reflector, the holographic surface measurements were conducted to receive a signal from a geosynchronous satellite orbiting just above the Shanghai city, which locates at azimuth angle 180degree and the elevation 52degree. The result is shown in Fig. 5 and at this fixed elevation angle we can see that the 65-m telescope has good surface accuracy of 0.32mm-rms. The surface accuracy is good enough in the highest observing frequency of 50GHz, one twentyth of the wavelength ($\lambda=6\text{mm}$).

2.2 A test 22-GHz receiver

The main reflector of the 65-m telescope has the potential surface accuracy of 0.32mm, which is confirmed by holographical surface measurement described in the previous section. It is necessary, however, to know the gravitational deformation at the different elevation angles. The holographical

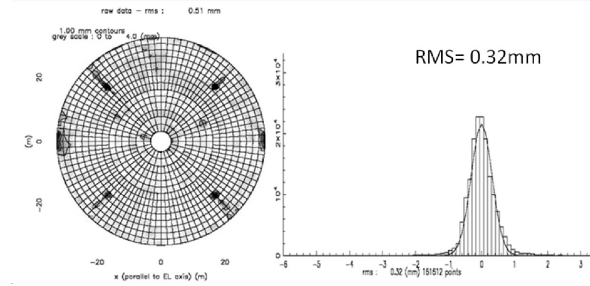


Figure 5. The Tian Ma 65m telescope

surface measurements by using a celestial strong masers as a reference signal are planned. The strongest water maser source, W49N, will be observed with two radio telescopes of 25-m and 65-m and the interferometer fringes will be analyzed to measure the surface accuracy of the 65-m telescope, which is scanned around the W49N while the 25-m telescope keeps tracking on the W49n at the center beam. For the W49N holography, a test 22-GHz receiver is prepared as shown in Fig.6. It is used under a room temperature environment but has enough performance to detect W49N with enough signal-to-noise ratio.

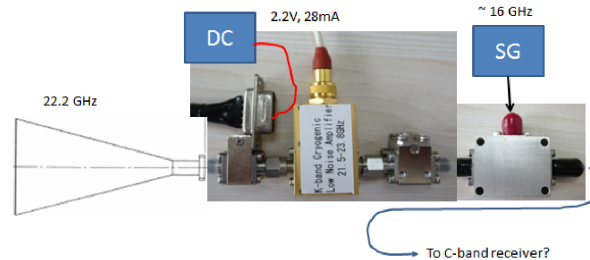


Figure 6. A configuration of a 22-GHz test receiver

The performance was tested and shown in Fig. 7 and Fig. 8.

2.3 Holographic Surface Measurement by a strong maser

The flux density of the W49N is confirmed with a VERA telescope and found to be 40KJy. The baseline sensitivity between 25-m and 65-m telescopes at Sheshan has well been estimated to be 2200Jy. The SNR of 8000 is expected with integration time of one second. The holography test with the dynamic range of more than 30dB is possible to do. The test result will be reported later.

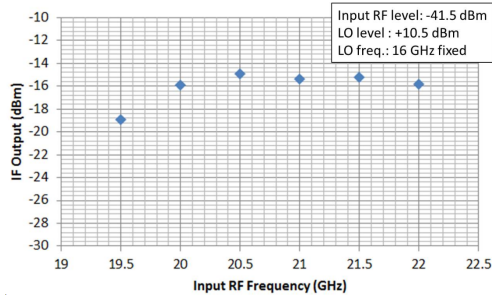


Figure 7. The system gain of an LNA and a mixer

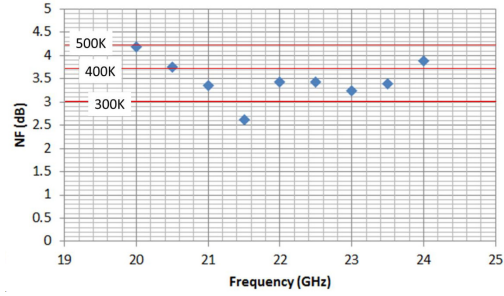


Figure 8. Noise performance at a room temperature environment

Acknowledgement

The LNA and the mixer was loaned by Japan Communication Equipment Co. Ltd.(Nihon-Tsusinki). Also I got many supports from the staffs in Shanghai Observatory.I would like to express my great thanks to the company and colleagues in Shanghai Observatory. The data of the satellite holography was provided by Dr. Wang Jinqing. Great thanks to him.

Status of Broadband VLBI Observation System (Gala-V) Development

Mamoru Sekido(sekido@nict.go.jp),
K. Takefuji, H. Ujihara, M. Tsutsumi,
S. Hasegawa, Y. Miyauchi, E. Kawai,
R. Ichikawa, Y. Koyama, and T. Kondo

*NICT Space-Time Standards Laboratory,
Kashima Space Technology Center,
893-1 Hirai, Kashima Ibaraki, Japan*

Abstract: The Gala-V is a broadband VLBI system composed of two small diameter antennas and large diameter one for precise time and frequency transfer over intercontinental distances. The prototype of the broadband feed for the Gala-V has been newly designed for the 34m radio telescope. First light observation has been successfully made as simultaneous observation of 6.7GHz and 12.2GHz Methanol maser line spectrum from W3OH in January 2014. Pair of small diameter antenna MARBLE1 (1.6m diameter) and MARBLE2 (1.5m diameter) are ready for broadband observation with single linear polarization. The MARBLE1 antenna has been moved to National Metrology Institute of Japan (NMIJ) at Tsukuba in March 2014. Since both the NMIJ and NICT are time keeping laboratory of UTC(k), thus time comparison between NICT and NMIJ is good test bed for evaluation of the time comparison techniques. Three sessions of 24 hours geodetic VLBI experiments were conducted in April - May 2014, and their station coordinates are determined within 5 mm horizontal and within 5cm in vertical repeatability.

1. Introduction

Counting microwave frequency emitted from Cs atoms is used for standard unit of length of time at present. More accurate clock based on counting optical emission from particular atoms are investigated and will become atomic time standard in the next generation(e.g.[1]). For establishing re-definition of second, precise frequency comparison between laboratories over intercontinental distances is required. For the purpose of distant frequency comparison, we are developing transportable broadband VLBI system (Gala-V). The data acquisition of the system is made by acquiring signal of 4 bands of 1 GHz width each in the frequency range of 3.2–14 GHz. Fixed frequency array is designed in the Gala-V at present, and the frequency array is selected based on (1) RFI survey and (2) minimum redundancy array for high delay resolution [2]. Although the frequency array is tentatively fixed in our project whereas flexible choice of the band is specification of VGOS[3], compatibility with the VGOS observing system is always in



Figure 1. Prototype of Iguana Feed install at Kashima 34m antenna. SEFD is 1000 – 1500 Jy in 6.5–14 GHz frequency range.

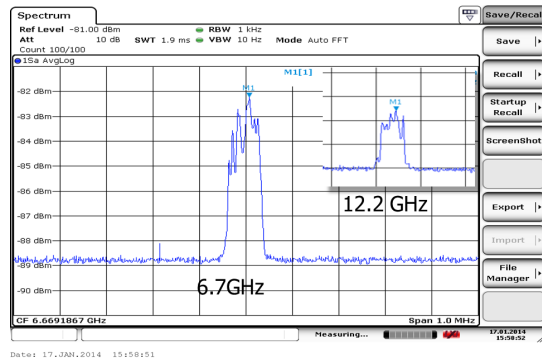


Figure 2. Frequency Spectra 6.7GHz and 12.2 GHz of Methanol maser source W3OH observed with Iguana prototype Feed of Kashima 34m antenna.

mind. Following section describes the progress of broadband system development and time and frequency transfer project since the last issue of TDC News[2].

2. Broadband system Development

Known broadband feeds such as eleven feed[4] and QRFH[5] have wide beam size, thus we had to develop new broadband feed for our Cassegrain type 34 m antenna, whose viewing angle from the focal point to the sub reflector is 34 degrees wide. The first prototype of the broadband feed (Named 'Iguana Feed') developed by NICT, whose frequency range is 6.5–14GHz, was installed in Dec. 2013(Fig.1). The first light observation was successfully made in January 2014, where two emission lines of methanol maser at 6.7 GHz and 12.2 GHz were simultaneously observed from the radio source W3OH(Fig.2). Current system equivalent flux density of the broadband system of Kashima 34m antenna is 1000–1500 Jy in 6.5–14GHz range. Though this feed will be used by the end of 2014 for



Figure 3. MARBLE1 station installed at the top of 3-7 building of NMIJ at Tsukuba.

evaluation, upgrade of the feed design is under the plan to enable 3.2–14 GHz observation with better efficiency.

3. Moving MARBLE1 to Tsukuba (NMIJ)

The Gala-V system is composed of pair of small antennas and Kashima 34m telescope. Two small antennas (MARBLE1 and MARBLE2) have prime focus parabolic antenna with 1.6 m and 1.5 m diameter dishes, respectively. Quad Ridge Horn Antenna (QRHA)[6] is used for the feed, and has been ready for broadband single linear polarization observation. The MARBLE2 antenna has been installed at the top of the second building of NICT headquarters at Koganei. The MARBLE1 antenna was moved from Kashima Space Technology Center (KSTC) to National Metrology Institute of Japan (NMIJ) at Tsukuba in the end of March 2014 (Fig.3). Both NICT and NMIJ have been keeping their own time scale by atomic time standards, and their UTC(k) are regularly compared with UTC determined by the BIPM (Bureau International des Poids et Mesure). Therefore time comparison between NICT (Koganei) and NMIJ (Tsukuba) is a good test-bed for development of frequency comparison technique. After installation of MARBLE1 to NMIJ(Tsukuba), 24 hours geodetic VLBI experiments were conducted three times with X-band.

Table 1. Station coordinates determined by five VLBI experiments (22-13 April 14-15 May, 30-31 May, 26-27 Jun., and 1-3 Aug.). Station Coordinates are estimated with Kashima 34m station coordinates fixed. Its epoch is MJD=56808.0.

Station	XYZ [mm]	σ_{err} [mm]	
MARBLE1 (Tsukuba)	X	-3962276706.9	8
	Y	3308884000.7	10
	Z	3733538093.0	6
MARBLE2 (Koganei)	X	-3942062034.9	6
	Y	3368277053.9	7
	Z	3702003875.0	8
(Fixed) KASHIM34	X	-3997650058.0	
	Y	3276690071.0	
	Z	3724278461.0	

Table 1 shows the station coordinates determined by 34m antenna station coordinates fixed.

4. Three station experiments and frequency Comparison

Since baseline of small diameter antenna pair does not have enough sensitivity, VLBI data of AB baseline was formed by linear combination of observable of OA,OB baseline, where A:MARBLE1, B:MARBLE2, O:KASHIM34. The converting from two baseline data of OA,OB to single baseline AB data is given by following equation:

$$\begin{aligned}
 \tau_{AB}(t_{\text{prt}}) &= \tau_{OB}(t_{\text{prt}} - \tau_{OA}(t_{\text{prt}})) - \tau_{OA}(t_{\text{prt}} - \tau_{OA}(t_{\text{prt}})) \\
 &\cong \tau_{OB}(t_{\text{prt}}) - \tau_{OA}(t_{\text{prt}}) - \tau_{AB}(t_{\text{prt}})\tau_{OA}(t_{\text{prt}})
 \end{aligned}$$

where t_{prt} is Epoch of data to be analyzed. Latter equation is expression of the first order approximating with respect to τ_{OA} with observed values τ_{OA}, τ_{OB} and computed values of τ_{AB} . This equation has precision better than 1 pico second on any ground based VLBI observation.

By using the geodetic VLBI data in April and May, clock difference between NICT and NMIJ was examined. Clock difference estimated by using VLBI, GPS, and difference of UTC(k) published from BIMP¹ are displayed in Fig. 4. Vertical position of the GPS and VLBI data in the plot are indicated with offsets to be in the same range with UTC rapid and final data of the BPIM. These plots demonstrating that VLBI and GPS have similar performance on clock rate comparison and both data shows good agreement with the difference of UTC(k) rate reported from BIPM. Although this equation is neglecting the source structure effects, there are no significant problem at present because of relatively short baseline.

¹<http://www.bipm.org/jsp/en/TimeFtp.jsp?TypePub=publication>

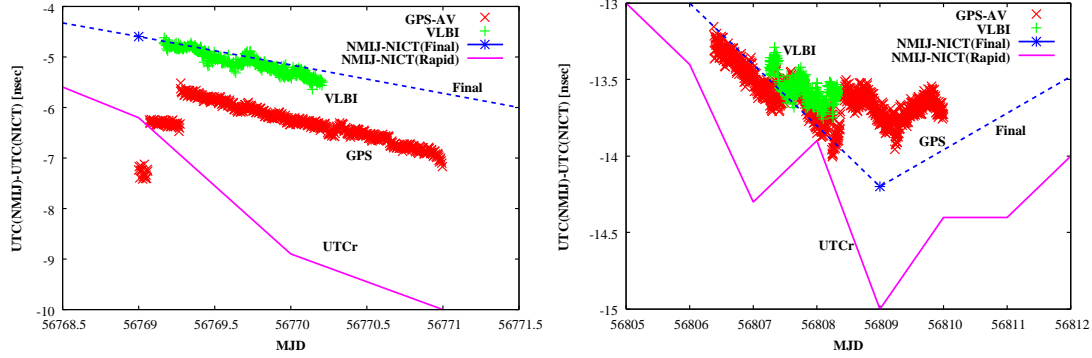


Figure 4. Clock comparison between UTC(NMIJ)- UTC(NICT) via VLBI(‘+’) and GPS(‘×’). Rapid UTC comparison UTCcr and final UTC(k) comparison data published from BIPM are over plotted with solid and dashed lines, respectively. Left panel is data during 22-24 Apr. and right panel is from 29th May to 2nd Jun.

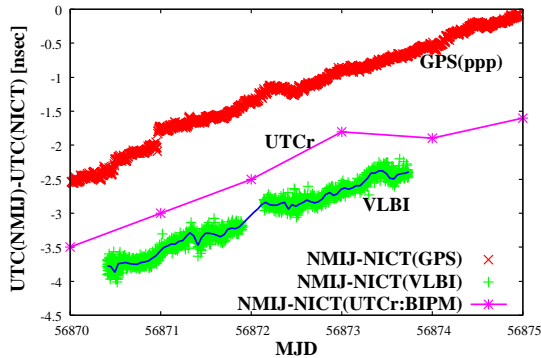


Figure 5. Clock comparison via VLBI(‘+’) and GPS(‘×’) performed during 1 – 3rd Aug. Vertical position of the GPS and VLBI plots are adjusted by arbitrary offset.

Continuous VLBI experiment for frequency comparison was conducted during 1st - 3rd of August. The clock data estimated by VLBI observation, GPS, and UTCcr data provided from BIPM were displayed in Fig.5. As the same with the results of Apr. - May, it is confirming that the VLBI analysis gives the consistent results with others. The scattering of the VLBI data is slightly larger than GPS in this experiment. Since the VLBI data is not always obtained in uniform interval, then statistics such as Allan variance is not applicable. Other statistical evaluation such as sigma-z[7] have to be considered.

Acknowledgments

We thanks to Dr. K. Watabe, Dr. T. Suzuyama, and Dr. M. Amemiya of NMIJ for supporting the VLBI experiment and the collaboration. We acknowledge Prof. K. Fujisawa of Yamaguchi University, Dr. M. Honma, and Dr. N. Matsumoto of National Astronomical Observatory for supporting broadband feed development.

References

- [1] Gill P., “When should we change the definition of the second?”,Phil. Trans. R. Soc. A, 369, doi: 10.1098/rsta.2011.0237,2011.
- [2] Sekido, M., et al., Development of Wide-band VLBI system (Gala-V), IVS NICT-TDC News No. 33, 11-14, 2013.
- [3] Bill Petrachenko, VLBI2010: Progress and Challenges, IVS 2012 General Meeting Proceedings, 42-46 2012.
- [4] Yang J., et al., “Cryogenic 2-13 GHz Eleven Feed for Reflector Antennas in Future Wide-band Radio Telescopes” IEEE Trans. Ant. & Prop., Vol. 59, NO. 6, pp.1918-1934, 2011.
- [5] Akgiray A., et al., “Circular Quadruple-Ridged Flared Horn Achieving Near-Constant Beamwidth Over Multioctave Bandwidth: Design and Measurements” IEEE Trans. Ant. & Prop., Vol. 61, NO. 3, pp.1099-1108, 2013
- [6] V. Rodriguez, “A multi-octave open-boundary quadridge horn antenna for use in the S to Ku-bands,Microwave Journal, March, pp. 84-92, 2006.
- [7] Matsakis D., and Josties F. J., “Pulsar-Appropriate Clock Statistics”, ADA419480. 28th Annual Precise Time and Time Interval (PTTI) Applications and Planning Meeting, Reston, VA, 3-5 Dec 1996.

Development of digital filters toward GHz-width VLBI

Kazuhiro Takefuji (*takefuji@nict.go.jp*),
Mamoru Sekido, Hideki Ujihara,
Masanori Tsutsumi, Shingo Hasegawa,
and Tetsuro Kondo

*Kashima Space Technology Center,
National Institute of Information
and Communications Technology,
893-1 Hirai, Kashima, Ibaraki 314-8501, Japan*

Abstract: We have been studying a frequency comparison technique with VLBI between 34 m in Kashima, Ibaraki and two 1.5 m compact antennas located in Koganei, Tokyo and in Tsukuba, Ibaraki, respectively. Therefore, it is necessary to have a broad-band system to get better signal to noise ratio because of the compact antenna smallness. To improve the performance of VLBI between the compact antennas and Kashima 34 m, we have developed digital filters using a signal processor of ADS3000+. Here we describe the techniques of digital equalizer to compensate a steep band-pass profile and digital band-pass filter for a VLBI observation of a maser.

1. Introduction

National Institute of Information and Communications Technology (NICT) has been not only developing VLBI observation system as the IVS-TDC, but also maintenance and keep the Japanese time standard. Recently NICT, AIST and Tokyo university have been developing an optical-lattice clock for the next generation time standards and for the redefinition of "the Second". Thus, it is necessary to compare the distant clocks somehow with several techniques. If two stations are close in a few hundreds kilometer, optical-fiber transmission [4] is the best technique for the comparison. However distant stations comparison over thousand kilometer and inter-continent is needed some technique through space for example GPS, Two-Way Satellite Time and Frequency Transfer (TWSTFT) and VLBI.

As for the Time and Frequency transfer (T&F) by VLBI, the order of 10^{-16} in a few days is targeted. Since our two compact 1.5 m antennas are quite small for VLBI, it is necessary to have a broad-band system such as a VLBI2010 Global Observing System (VGOS).

For the next generation of the geodetic VLBI, VGOS has been specified a fast moving antenna and broad-band receivers. Some antennas, which

meet the VGOS requirements, have been constructed for example GGAO 12 m antenna and 18 m Westford in the United States, TWIN Radio Telescope Wettzell (TTW) in Germany, the RAEGE telescope at Yebes in Spain and Ishioka telescope in Japan.

We, NICT/Kashima, has been also developing a broad-band system from 3 GHz to 15 GHz to our Kashima 34 meter antenna and two small/transportability antennas. The broad-band project is named "Gala-V". The most different things from other VGOS antenna, first we use a 30 m class antenna, a feed horn (proto-type No.2) was installed on December 2013, has a sharp beam pattern of 12 degree to illuminate the sub-reflector. Moreover, We decided that no-redundant frequency array of 3.2 GHz, 4.8 GHz, 9.6 GHz, 12.8 GHz is fixed. This array has fine delay resolution with minimum side-lobes and the array is got int line straightly in case of sampling speed at 16 GHz without DBBC. [1].

Out two compact antennas have 1.5 and 1.6 m diameter, thus it is not easy to obtain fringes.

2. Digital signal processing for the broad-band receiver

Figure 1 shows an internal signal flow of ADS3000+[3]. Two Intermediated frequency (IF) signals are sampled simultaneously at speed of 2048MHz and 8-bits quantization. Then, Finite Impulse Responce filter (FIR), whose coefficient are manually loaded through LAN-based telnet, are applied to sampled stream in real-time. If the coefficient of the FIR is made within 65 taps, any designs of the filter such as low-pass, high-pass, band-pass, band-rejection and equalizer are possible to realize. ADS3000+ has other FPGA core of the digital base-band conversion, a comaprison test between other Digital-Backend (DBE) was reported by Whitney [5].

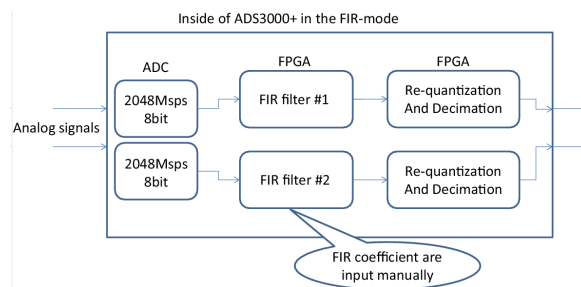


Figure 1. Signal flow of ADS3000+, FPGAs realize any FIR filters.

2.1 Digital equalizer

Since our vlbi experiment are carried out over 1 GHz bandwidth, a band-profile has a difficulty to keep flat. For the purpose of the band-profile to be flat, We made a digital equalizer to compensate a bad band-profile. Actually the digital equalizer is made by a “bad-profile” itself. Firstly we take that spectrum as a template. Secondly we make a matched filter by inverting the template. Thirdly a coefficient of FIR completes after the matched filter converts into 8-bits length. A wider bit length has wider dynamic range. Equation 5 shows the relationship between dynamic range (here it is same as SNR) and bit length [6],

$$SNR = 6.02N + 1.76[dB], \tag{5}$$

where N is bit length. Since ADS3000+ has a dynamic range of 50 dB ($6.02*8+1.76$), the realized digital filter becomes also high dynamic range even 1 or 2-bits re-quantization. Figure 2 shows before and after the applied digital equalizer. A 10 dB difference on the X-band of the 34 m could be reduced to a few dB. There are still some ripples on the band-profile. However, the ripple must be much flat when the number of the coefficient tap can increase.

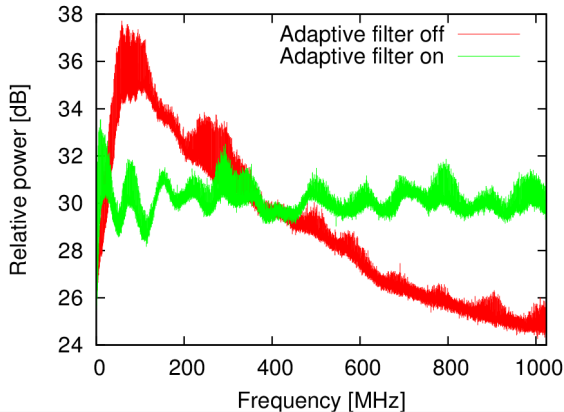


Figure 2. The digital equalizer is demonstrated to X-band of the Kashima 34 m.

Then we carried out VLBI observation for the digital equalizer between the compact antenna and Kashima 34 m. Figure 3 and 4 show the results. A effect of the digital equalizer can be seen on the cross-spectrum even the VLBI. The cross-spectrum of the figure 4 became much flat comparing with figure 3. The SNR of the fringes also increased the strength of 20 % with three times on-off operations. Therefore, We could use the sampling bits with flat spectrum much effectively.

2.2 Digital band-pass filter

In case of observing a maser source with wide-band VLBI, RFI signals become major issues. To suppress the RFI, we realize a digital band-pass filter with ADS3000+. We make the digital BPF, which focused on a spectral line 6.7GHz of methanol maser emission.

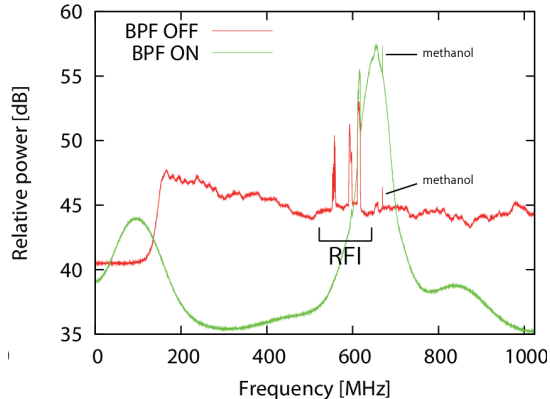


Figure 5. The digital band-pass filter is demonstrated the spectral line of methanol maser. Dynamic range was slightly improved when digital BPF was applied.

Figure 5 shows the on-off operation of the digital BPF. Most RFI could be removed. Moreover, dynamic range of the maser line (ground level-to-peak) increased 1.65 dB to 2.23 dB. Since the time difference of the on-off operation was only 2 min, we considered that the improvement was caused by effective sampling. We carried out the maser source observation between the compact antenna and Kashima 34 m

3. Summery

We have been developed the digital equalizer and digital band-pass filter to improve a performance of VLBI and to suppress RFIs. Since the digital equalizer compensates the band-profile to be flat, we could obtain better fringes. The digital BPF suppressed the RFI and we could focus on the spectral line of the maser emission which becomes slightly wide dynamic range. The other digital filter can be created to satisfy other requirements.

References

[1] Mamoru Sekido, Kazuhiro Takefuji, Hideki Ujihara, Thomas Hobiger, Masanori Tsutsumi, Shingo Hasegawa, Yuka Miyauchi, Ryuichi Ichikawa, Yasuhiro Koyama, and Tetsuro Kondo, Development of Wide-band VLBI

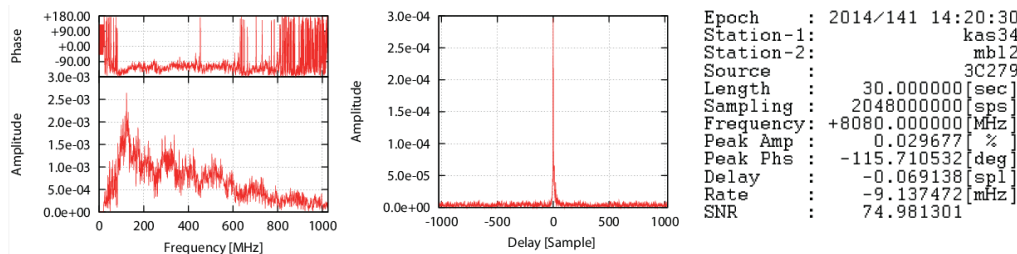


Figure 3. Result of a VLBI experiment without the digital equalizer

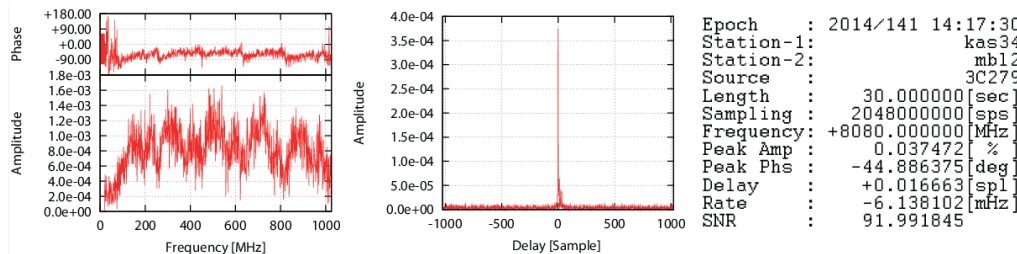


Figure 4. Result of a VLBI experiment with the digital equalizer. The SNR was improved about 20 %.

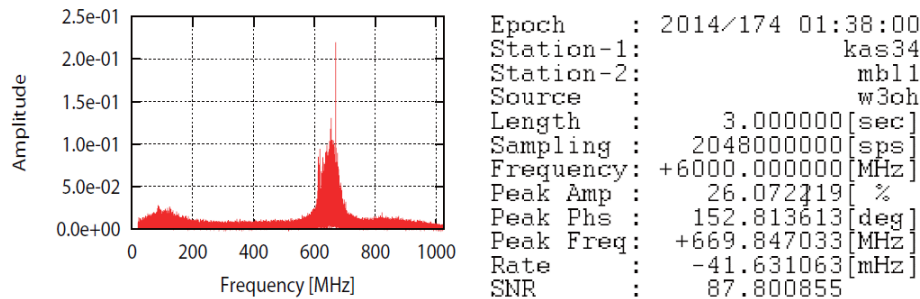


Figure 6. Result of VLBI with digital BPF. RFIs could be suppressed outside the bandwidth of the BPF.

- system (Gala-V), IVS NICT-TDC News No. 33, 2013.
- [2] Mamoru Sekido, K. Takefuji, H. Ujihara, M. Tsutsumi, S. Hasegawa, Y. Miyauchi, E. Kawai, R. Ichikawa, Y. Koyama, and T. Kondo, Status of Broadband VLBI Observation System (Gala-V) Development, IVS NICT-TDC News No. 34, 2014.
 - [3] Kazuhiro Takefuji, Masanori Tsutsumi, Hiroshi Takeuchi, Yasuhiro Koyama, Current Status of Next Generation A/D Sampler ADS3000+, IVS NICT-TDC News No.31, 2010.
 - [4] M.Fujieda, M.Kumagai, S.Nagano, Coherent microwave transfer over a 204-km telecom fiber link by a cascaded system, IEEE TUFFC, vol.57, no.1, pp.168-174, 2010.
 - [5] Alan Whitney, Chris Beaudoin, Roger Cappallo, Arthur Niell, Bill Petrachenko, Chester A. Ruzszyk, and Mike Titus, VLBI Digital-Backend Intercomparison Test Report, "http://www.haystack.mit.edu/workshop/ivtwp/2012.12.17_DBE_testing_memo_final.pdf"
 - [6] Walt Kester, "Understand SINAD, ENOB, SNR, THD, THD + N, and SFDR so You Don't Get Lost in the Noise Floor", http://www.analog.com/static/imported-files/tutorials/MT-003.pdf

On a Wide-Band Bandwidth Synthesis

Testuro Kondo (*kondo@nict.go.jp*)
and Kazuhiro Takefuji

*Kashima Space Technology Center,
National Institute of Information
and Communications Technology,
893-1 Hirai, Kashima, Ibaraki 314-8501, Japan*

1. Introduction

The bandwidth synthesizing software named “KOMB” is a software package to obtain delay residual and delay rate residual from cross-correlation data [Kondo and Kunimori, 1984; Kondo et al., 1999]. KOMB was initially developed for treating the correlated data consisting of a number of channels (14 or 16) where each channel has a narrow frequency bandwidth of 2 – 32 MHz and is distributed in dual RF bands (S-band (2 GHz) and X-band (8 GHz)).

Recently it becomes possible to sample signals with a sampling frequency of 1024 MHz (corresponding to 512MHz bandwidth) and higher because of a remarkable progress in the performance of a sampling device. Now a wide band observation system exceeding a band width of 10 GHz is under the development. The current version of KOMB cannot process such wide-band observation data. We are, therefore, investigating a realistic method to obtain delay residual and delay rate residual from wide-band data to revise the software KOMB.

2. Search function

A “coarse search” and a “fine search” were initially developed by Whitney [1974] and have been used for long time to obtain delay and delay rate residuals from correlated data.

2.1 Coarse search function

Eq.(6) shows the integration of a cross-spectrum $S(f, t)$ over time t and frequency f with correcting a trial phase θ for a cross-spectrum. This equation is called a search function, and a θ which maximizes $F(\theta)$ is a solution, i.e., a search result.

$$F(\theta) = \left| \int \int S(f, t) \exp\{-i\theta\} df dt \right| \quad (6)$$

When θ is expressed by using a residual delay ($\Delta\tau$) and a residual delay rate ($\Delta\dot{\tau}$) as follows,

$$\theta = 2\pi f(\Delta\tau + \Delta\dot{\tau}t), \quad (7)$$

eq.(6) can be written as

$$F(\Delta\tau, \Delta\dot{\tau}) = \left| \int_{t_0}^{t_1} \int_{f_0}^{f_0+f_B} S(f, t) \cdot \exp\{-i2\pi f(\Delta\tau + \Delta\dot{\tau}t)\} df dt \right|. \quad (8)$$

Changing an integration range for frequency from $f_0 \sim f_0+f_B$ to $0 \sim f_B$, i.e., introducing $f_v = f - f_0$, eq.(8) can be re-written as

$$F(\Delta\tau, \Delta\dot{\tau}) = \left| \exp(-i2\pi f_0\Delta\tau) \cdot \int_{t_0}^{t_1} \int_0^{f_B} S(f_v, t) \exp(-i2\pi f_v\Delta\tau) \cdot \exp(-i2\pi f_0\Delta\dot{\tau}t) \exp(-i2\pi f_v\Delta\dot{\tau}t) df_v dt \right| \quad (9)$$

Here, $|\exp(-i2\pi f_0\Delta\tau)| \equiv 1$ and the last term $\exp(-i2\pi f_v\Delta\dot{\tau}t)$ is considered as 0 under the condition of conventional VLBI observation, i.e., $f_B \sim 10$ MHz and $t_1 \sim 100$ sec. Finally, we get

$$F(\Delta\tau, \Delta\dot{\tau}) = \left| \int_{t_0}^{t_1} \left\{ \int_0^{f_B} S(f_v, t) \cdot \exp(-i2\pi f_v\Delta\tau) df_v \right\} \cdot \exp(-i2\pi f_0\Delta\dot{\tau}t) dt \right|. \quad (10)$$

Eq.(10) is a two-dimensional (2-D) Fourier transform with respect to $\Delta\tau$ and $f_0\Delta\dot{\tau}$, so we can use a 2-D fast Fourier transform (FFT) to calculate the search function.

2.2 Fine search function

A bandwidth synthesis combines a number of channels. A search function of a bandwidth synthesis is defined as

$$F(\Delta\tau, \Delta\dot{\tau}) = \left| \sum_{n=1}^N \int_{t_0}^{t_1} \int_0^{f_B} S_n(f_v, t) \cdot \exp[-i\{2\pi(f_n + f_v)\Delta\tau + \phi_n\}] \cdot \exp\{-i2\pi(f_n + f_v)\Delta\dot{\tau}t\} df_v dt \right| \\ \approx \left| \sum_{n=1}^N \exp(-i2\pi f_n\Delta\tau) \cdot \int_{t_0}^{t_1} \int_0^{f_B} S_n(f_v, t) \exp\{-i(2\pi f_v\Delta\tau + \phi_n)\} \cdot \exp(-i2\pi f_n\Delta\dot{\tau}t) df_v dt \right| \quad (11)$$

where a frequency range for channel n is $f_n \sim f_n + f_B$ and ϕ_n is an additional instrumental phase

at each channel, and $\exp(-i2\pi f_v \Delta \dot{t}) \approx 0$ is assumed again. Let $\Delta\tau = \Delta\tau_m + \Delta\tau_s$ and $\Delta\dot{\tau} = \Delta\dot{\tau}_m + \Delta\dot{\tau}_s$ where $\Delta\tau_s$ and $\Delta\dot{\tau}_s$ corresponds to the residual obtained by the coarse search and assuming $|2\pi f_v \Delta\tau_m| \ll 1$, eq.(11) can be re-written as

$$F(\Delta\tau, \Delta\dot{\tau}) = \left| \sum_{n=1}^N \exp(-i2\pi f_n \Delta\tau) \cdot \int_{t_0}^{t_1} \left(\int_0^{f_B} S_n(f_v, t) \cdot \exp\{-i(2\pi f_v \Delta\tau_s + \phi_n)\} df_v \right) \cdot \exp(-i2\pi f_n \Delta\dot{\tau}_s t) \cdot \exp(-i2\pi f_n \Delta\dot{\tau}_m t) dt \right|. \quad (12)$$

We, now, define $D_s(n, t)$ as

$$D_s(n, t) = \exp(-i\phi_n) \left(\int_0^{f_B} S_n(f_v, t) \cdot \exp(-i2\pi f_v \Delta\tau_s) df_v \right) \cdot \exp(-i2\pi f_n \Delta\dot{\tau}_s t), \quad (13)$$

then we have

$$F(\Delta\tau, \Delta\dot{\tau}) = \left| \sum_{n=1}^N \exp(-i2\pi f_n \Delta\tau) \cdot \int_{t_0}^{t_1} D_s(n, t) \exp(-i2\pi f_n \Delta\dot{\tau}_m t) dt \right|. \quad (14)$$

Eq.(14) can be re-written as

$$F(\Delta\tau, \Delta\dot{\tau}) = \left| \sum_{k=1}^K \left(\sum_{n=1}^N D_s(n, k) \cdot \exp(-i2\pi f_n \Delta\tau) \right) \cdot \exp(-i2\pi f_n \Delta\dot{\tau} \Delta tk) \right| \quad (15)$$

where $k(= 1, 2, \dots, K)$ is an index number in the time domain, Δt is its interval period, and $\Delta\dot{\tau}$ is now used instead of $\Delta\dot{\tau}_m$. Eq.(15) is called a fine search function. By using the lowest RF frequency f_1 , eq.(15) can be further re-written as

$$F(\Delta\tau, \Delta\dot{\tau}) = \left| \sum_{k=1}^K \left(\sum_{n=1}^N D_s(n, k) \cdot \exp(-i2\pi f_n \Delta\tau) \right) \cdot \exp(-i2\pi f_1 \Delta\dot{\tau} \Delta tk) \cdot \exp\{-i2\pi(f_n - f_1) \Delta\dot{\tau} \Delta tk\} \right|. \quad (16)$$

If $2\pi(f_n - f_1) \Delta\dot{\tau} \Delta tk \ll 1$, eq.(16) can be expressed as

$$F(\Delta\tau, \Delta\dot{\tau}) = \left| \sum_{k=1}^K \left(\sum_{n=1}^N D_s(n, k) \cdot \exp(-i2\pi f_n \Delta\tau) \right) \cdot \exp(-i2\pi f_1 \Delta\dot{\tau} \Delta tk) \right|. \quad (17)$$

Eq.(17) is a two-dimensional (2-D) Fourier transform with respect to $\Delta\tau$ and $f_1 \Delta\dot{\tau}$, so we can use a 2-D FFT again to calculate this function.

2.3 Condition for 2-D FFT

A 2-D FFT cannot be used for calculating a fine-search function when $|2\pi(f_n - f_1) \Delta\dot{\tau} \Delta tk| \ll 1$ is not satisfied. Let's investigate a condition allowed to use a 2-D FFT. Assuming an X-band, let a bandwidth be 1 GHz (i.e., $f_n - f_1 = 1$ GHz), and integration time $\Delta tk (= T)$ be 100 sec, then solving the condition

$$|2\pi(f_n - f_1) \Delta\dot{\tau} T| \ll 1 \quad (18)$$

regarding $\Delta\dot{\tau}$, we get the condition as follows.

$$|\Delta\dot{\tau}| \ll \frac{1}{2\pi(f_n - f_1) \Delta\dot{\tau} T} \approx 1.6 \times 10^{-12} \text{ (s/s)} \quad (19)$$

Namely, residual delay rate must be sufficiently less than 1.6×10^{-12} (s/s) to use an FFT. If in the case of a residual delay rate of about 1.6×10^{-12} (s/s), this is often occurred in an actual observation, a bandwidth should be sufficiently smaller than 1 GHz.

Actual processing in KOMB is performed as follows. At first, a coarse-search is carried out. Followed by coarse search results are reflected to cross spectra through eq.(13), and then a fine-search, i.e., a bandwidth synthesis is carried out. Hence rate residual at the bandwidth synthesis is thought to be close to zero. Thus we can use an FFT for calculating a fine-search function in the time domain. Although if there exists a large rate residual, an error due to this rate residual can be avoided, because a final calculation to find out a peak is carried out by calculating a search function directly (without use of an FFT).

When rate residual is sufficiently small to satisfy the condition discussed above, considering f_B in eq.(10) as a total bandwidth of an X-band and using the sufficient number of FFT points in a frequency domain, it is possible to carry out a bandwidth synthesis by a 2-D FFT without a coarse-search process. When KOMB was developed, the number of FFT points suitable for practical use was limited to at most 8192 or so. It was, therefore,

unable to execute a bandwidth synthesis without a coarse-search process efficiently at that time. So that, a search process was divided into two steps, such as a coarse-search and a fine-search. However, it was a quite reasonable processing method considering from the case that large rate residual remained.

The discussion so far is the case considering a bandwidth of at most 1 GHz. If we consider the case of a bandwidth of up to several GHz with an ionospheric delay, how a search function can be expressed?

3. Wide band search function

In order to discuss a search function in the case of wide band under the existence of ionospheric delay, eq.(7) is modified as

$$\theta = 2\pi f \{ \Delta\tau + \Delta\dot{\tau}t + \Delta\tau_{ion}(f) \} \quad (20)$$

where $\Delta\tau_{ion}(f)$ denotes an ionospheric delay and it is expressed as

$$\Delta\tau_{ion}(f) = \alpha f^{-2} \Delta D \quad (21)$$

for a frequency range sufficiently higher than the plasma frequency of ionosphere (≈ 10 MHz) [see, e.g., *Ratcliffe*, 1959], where ΔD is the difference of total electron content (TEC) in ray paths to two stations (unit is electron/m²), and $\alpha = \pm 1.34 \times 10^{-7}$ where a positive sign is for a group delay and negative for a phase delay.

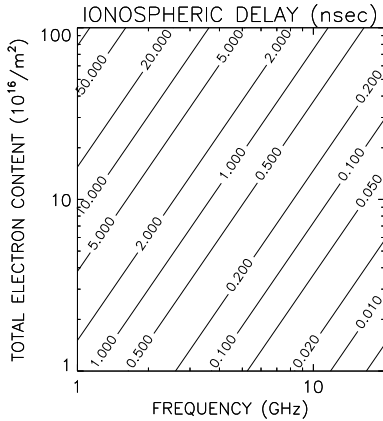


Figure 1. Relation between total electron content (TEC) and frequency for various ionospheric (group) delays.

Fig.1 shows a relation between total electron content (TEC) and frequency for various ionospheric (group) delays. For an example we can read from the figure that the difference of ionospheric delays between S-band (2GHz) and X-band

(8GHz) is about 3 nsec for the difference of TECs of $10^{17}/\text{m}^2$ (this TEC difference can occur sometimes). Using eq.(20), we can write a search function as

$$F(\Delta\tau, \Delta\dot{\tau}) = \left| \int_{t_0}^{t_1} \int_{f_0}^{f_1} S(f, t) \cdot \exp\{-i2\pi f(\Delta\tau + \alpha f^{-2} \Delta D)\} \cdot \exp(-i2\pi f \Delta\dot{\tau}t) df dt \right| \quad (22)$$

Now we assume a wide band such as from 2 GHz (f_0) to 14 GHz (f_1). In this case effect of ionosphere can no longer be neglected. Therefore we should use eq.(22) as a search function. In other words, it has the possibility of estimating TEC as well as a residual delay. However the frequency dependency of the term $\exp(-i2\pi f \Delta\dot{\tau}t)$ in the time direction becomes large, and it is difficult to adopt an FFT for calculating the integration in the time domain.

In the mean time, the term of frequency integral in eq.(22) is called a delay resolution function, i.e.,

$$D(\Delta\tau) = \int_{f_0}^{f_1} S(f) \cdot \exp\{-i2\pi f(\Delta\tau + \alpha f^{-2} \Delta D)\} df \quad (23)$$

Let's investigate an ionospheric effect on a wide-band observation by using the delay resolution function.

3.1 Examples of delay resolution function

Fig.2 shows an example of frequency allocation at a wide-band observation. Fig.3 shows the

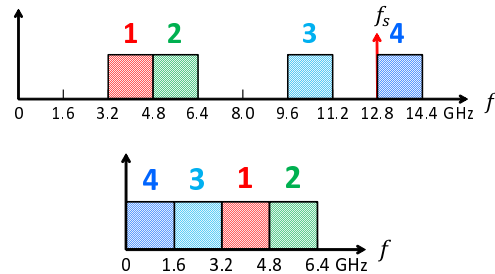


Figure 2. An example of frequency allocation at a wide-band observation (upper panel). The lower panel shows a frequency allocation after sampled with a sampling frequency of 12.8 GHz. As shown in the figure, the frequency allocation is a non-redundant allocation.

delay resolution function (eq.(23)) without ionosphere (i.e., $\Delta D = 0$) for the case of the frequency

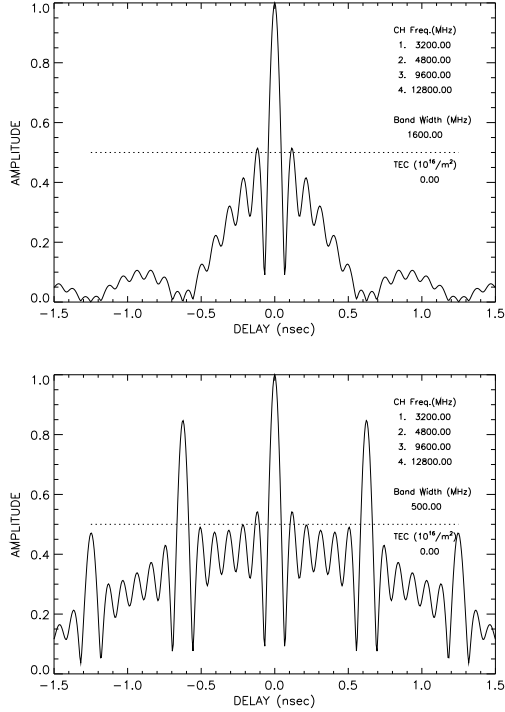


Figure 3. A delay resolution function without ionosphere (i.e., $\Delta D = 0$) for the frequency allocation given by Fig.2 for a bandwidth of 1.6 GHz (upper) and for 0.5 GHz (lower). In case of 0.5 GHz bandwidth, an ambiguity of 0.625 nsec appears caused by the least common multiple of frequency spacing (1.6 GHz) of each band.

allocation given by Fig.2 and for bandwidths of 1.6 GHz and 0.5 GHz for each frequency channel (band). In case of 0.5 GHz bandwidth, an ambiguity of 0.625 nsec appears caused by the least common multiple of frequency spacing (1.6 GHz).

Fig.4 shows the case of a TEC of $4.0 \times 10^{16} \text{el/m}^2$. The shift of the main peak occurs. Moreover, symmetry of the function is lost and a larger peak appears at a position different from the original delay position. Fig.5 shows the case for larger TEC ($10.0 \times 10^{16} \text{el/m}^2$: this situation can occur commonly). Peak amplitude is weakened by half for the case of a 1.6 GHz band width.

As shown in these examples, it is difficult to determine residual delay by calculating a delay resolution function. Furthermore, the frequency dependency of the term $\exp(-i2\pi f \Delta \dot{\tau} t)$ cannot be neglected for a large delay rate residual, then we cannot calculate a wide-band search function efficiently by using a 2-D FFT. In this case, what kind of a search method is realistic?

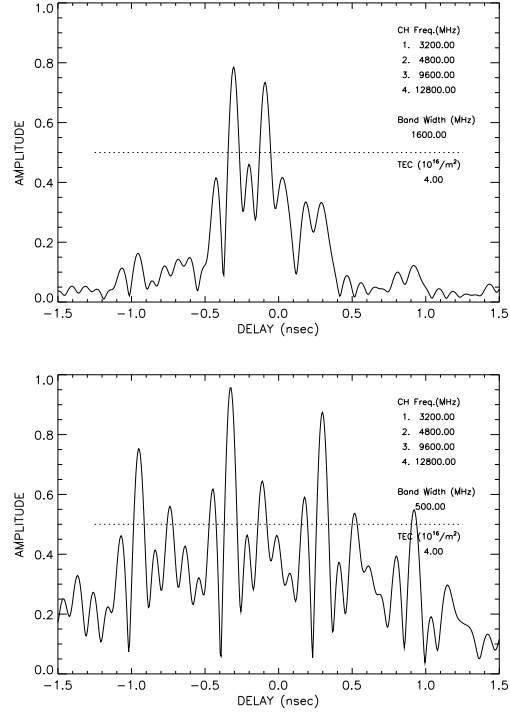


Figure 4. Same as Fig.3 for a TEC of $4.0 \times 10^{16} \text{el/m}^2$.

4. Realistic approach

4.1 Integration period available to use 2-D FFT

As have mentioned, we cannot use a 2-D FFT for calculating a search function in the case of a bandwidth of exceeding several GHz. However, an integration period of 100 sec has been assumed in the discussion. Thus, let's investigate the maximum integration period that 2-D FFT can be used for the calculation of a search function. A condition equation eq.(18) is shown below, but $f_n - f_1$ is replaced by f_B .

$$|2\pi f_B \Delta \dot{\tau} T| \ll 1 \quad (24)$$

Fig.6 shows a relation between delay rate residual ($\Delta \dot{\tau}$) and frequency range (bandwidth) (f_B) for various integration periods (T). Their relation satisfies the condition of $|2\pi f_B \Delta \dot{\tau} T| = 1$. For an example, we can read from the figure that in case of a bandwidth of 1.6 GHz an integration period is about 100 sec for $\Delta \dot{\tau}$ of 1 ps/s. This is derived from the condition of $|2\pi f_B \Delta \dot{\tau} T| = 1$, so that a band width should be small enough than 1.6 GHz to satisfy the condition of $|2\pi f_B \Delta \dot{\tau} T| \ll 1$ for the same integration period and rate residual. We can also read from the figure that $\Delta \dot{\tau}$ should be small enough than 1.6ps/s for the case of a bandwidth of

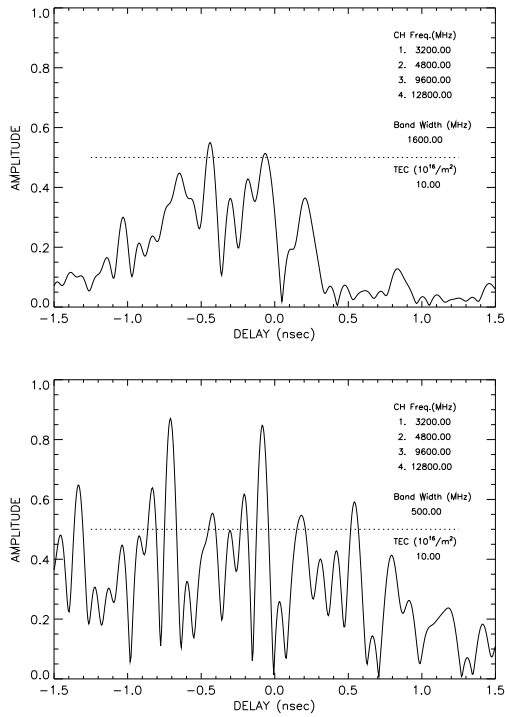


Figure 5. Same as Fig.3 for a TEC of $10.0 \times 10^{16} \text{el/m}^2$.

10 GHz and an integration time of 10 sec. If the condition is not satisfied, we cannot use a 2-D FFT for the calculation of a search function.

4.2 Realistic search method

Here we consider a realistic search method. The most realistic method is a two-step search that is conventionally carried out in the current version of KOMB, i.e., at first a coarse search, then followed by a fine search. Delay rate residual is determined by a coarse search under the condition of a bandwidth of at most 1 GHz (ionospheric effect is not so large unless $\Delta\dot{\tau}$ is not so large), and then a result is fed back to the correction of cross-spectra to calculate a wide-band search function by a 2-D FFT. If $\Delta\dot{\tau}$ is determined accurately enough at a coarse search process, rate search at a wide-band search can be omitted.

As for a fine delay search, two methods are considered as follows.

1. at first estimate TEC from each band results, then combine each band data with correcting ionospheric delays to obtain a fine delay.
2. calculate a delay resolution function directly for various combinations of TEC and delay, then find a peak to obtain a fine delay.

Method 1 will not work properly when a signal to noise ratio (SNR) of each band data is low. We

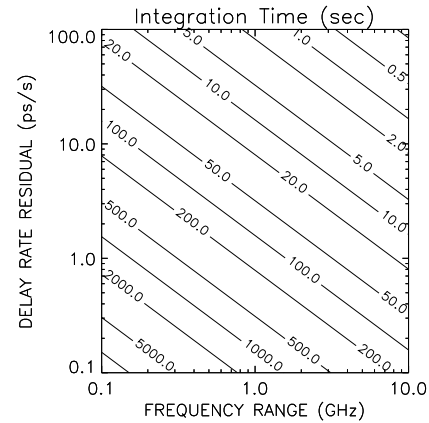


Figure 6. Relation between delay rate residual ($\Delta\dot{\tau}$) and frequency range (bandwidth) (f_B) for various integration periods (T) where their relation satisfies $|2\pi f_B \Delta\dot{\tau} T| = 1$.

can avoid this situation by scheduling an observation span length properly, so that we will develop a software program under the assumption that an SNR is assured for each band data.

5. Conclusion

Effects of delay rate residual and ionosphere on a wide-band bandwidth synthesis of which bandwidth reaches upto 10 GHz have been investigated. We have concluded that a two-step search consisting of a coarse search and a fine search is a realistic method so far, which is adopted in the current version of band width synthesizing software KOMB. However sufficient SNR at each band should be guaranteed to perform the search successfully. As for the case of insufficient SNR, we will continue to investigate a possible method.

References

Kondo, T. and H. Kunimori, III-5 bandwidth synthesizing software (KOMB), Rev. Radio Res. Lab., Vol.30, No.1, pp.199-216, 1984 (in Japanese).
 Kondo, T., M. Sekido, and H. Kiuchi, 3.2.3 KSP bandwidth synthesizing software, J. Commun. Res. Lab., Vol.46, No.1, pp.67-76, 1999.
 Ratcliffe, J.A., The magneto-ionic theory and its applications to the ionosphere, Cambridge University Press, 1959.
 Whitney, A.R., Precision geodesy and astrometry via very-long-baseline interferometry, Ph.D. Thesis, M.I.T., 1974.

Development of Wideband Feed

Hideki Ujihara (ujihara@nict.go.jp),
Kazuhiro Takefuji and Mamoru Sekido

Kashima Space Technology Center,
National Institute of Information
and Communications Technology,
893-1 Hirai, Kashima, Ibaraki 314-8501, Japan

1. Status of development

No other wideband feed fits for our antennas in beam size. Thus, two different types of wideband feeds were developed and now in production for Kashima 34m and MARBLE.

One was named IGUANA feed after our Gala-V (Galapagos VLBI) project in Kashima and aimed for cassegrain focus of conventional radio telescope with bandwidth of 2.2-18GHz (or 22GHz in plan). This feed is consisted with a smaller Daughter feed for higher frequency (above 6.5GHz) and bigger Mother feed for lower frequency (Fig.1).

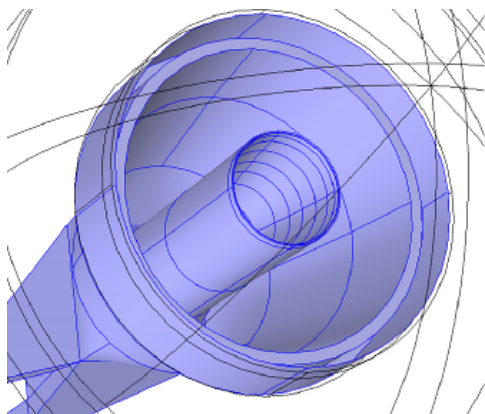


Figure 1. Simulation model of IGUANA feed in COMSOL Physical dimensions : $\phi 400\text{mm} \times L800\text{mm}$, more or less.

The daughter feed is a multimode horn (Fig.2), which realizes nearly same beam patterns in both E/H planes with low cross polar, without thick and complex wall structure in corrugated horn. Because it is placed in the mother feed, its wall should be thin, thus no choice for me. The two daughters were made as prototypes in early 2013 and tested in METLAB (Fig.3) and 34m antenna before the third and her Mom were designed. The second is resemble the first, but slim and its beam pattern is slightly fat.

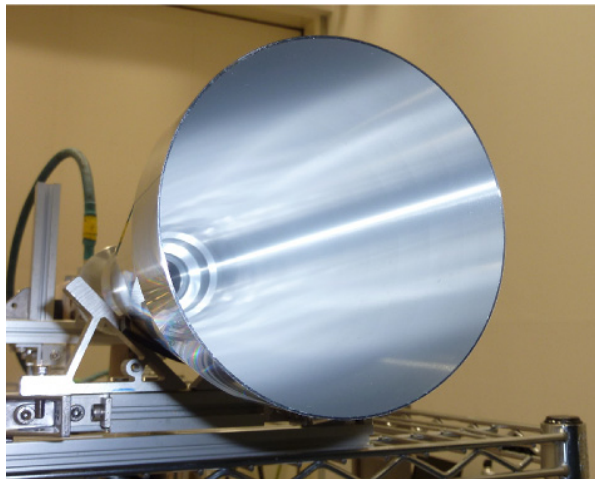


Figure 2. IGUANA daughter feed



Figure 3. Testing IGUANA daughter feed at MET-LAB in Kyoto UNIV. Physical dimensions are $\phi 133\text{mm}$ (No.1), $\phi 120\text{mm}$ (No.2) $\times L300\text{mm}$

Prototype feed No.1 were set on the place of previous C-Band horn (5GHz) of Kashima 34m in the end of 2013, then replaced by No.2, and they are tested and compared. Fringes of methanol masers (6.7/12.2GHz) were successfully obtained with MARBLE, which is small VLBI antenna with 1.5m or 1.6m diameter dish and its feed is placed at focus of parabola. IGUANA cannot stay on focus of MARBLE due to its size, thus another feed is needed. The other wideband feed has still no name, temporary here, it may be called as the new feed (Fig.4). The small one is for MARBLE and the other fat one is for 34m. They are designed for using at the center focus of parabola antenna, such as MARBLE or small antennas. However its beam size can be easily arranged for another optics. Gala-V uses 4 channels of 1.6GHz in 3.2-14.4GHz. They are 3.2-4.8GHz, 4.8-6.4GHz, 9.6-10.4GHz and 12.8-14.4GHz. This new feed can receive over 3.2-14.4GHz and its flat-head beam in higher channels will improve aperture efficiency of MARBLE without ring focus optics.

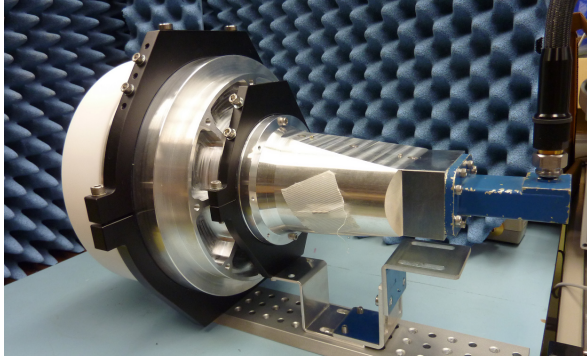


Figure 4.
New feed with WRD350D24-SMA output.
Physical dimensions : $\phi 240\text{mm} \times L300\text{mm}$

2. Numerical Simulation

Today, we can use 3D simulations for antenna design, but the simulator and computers do not give us the solution. The solution means a design of the antenna, which is defined as a problem of fixing each dimensions of every part of antenna structure to meet its specification, such as beam width, shape, return loss in every operational frequency.

Conventional feed, which is conical horn with or without corrugation, have very few design parameters, such as axial length, aperture diameter and input waveguide diameter...that's all, countable in a hand. However multimode horn or wideband feed has complex structure so it has much more physical parameters, thus the combination of the parameters will soon be greater than the numbers we can handle in our life. So heuristic choice of various ideas may be helpful. Before you dive into simulation, remember Chinese Postman Problem.

Also the choice of the numerical scheme affects in computational time. Iteration scheme take longer time for higher frequency because scales of the mesh against the wavelength become larger, thus declination rate of errors in each iteration steps become smaller. Fig.5 shows an example. Computational time for 12GHz is tenth longer than for 8GHz. However, this is efficient in memory size.

On the other hand, direct scheme offers nearly constant calculation time, however this is memory eater and its solution may have errors in higher frequency which may not be negligible. These are trade-off which you can choice. Highest frequency of the antenna defines resolution of the mesh and lowest defines antenna aperture size, thus simulations of whidband feed needs huge memories. In my case, typical simulation time for one model is a day, using 256GB physical memory...Let it Go! The heat of CPUs never bothered me anymore.

3. Measurements

3.1 Feeds

Far field beam patterns of the feeds were measured with near field scanner in METLAB of Kyoto Univ. IGUANA daughter feeds have circular waveguide output with nearly 6.4GHz cutoff frequency. We can use it with higher cutoff waveguide adaptor following SMA converter for single linear polarization output.

3.2 34m antenna

Measured T_{sys} and SEFD of 34m with No.2 prototype daughter feed are shown in Fig.6 and Fig.7 Aperture efficiency in Fig.8 was calculated from T_{sys} and SEFD. However it should be noted that is a preliminary result, T_{sys} is low at both of methanol frequencies, that is good for astronomers.

The aperture efficiency is around 40% due to offset of the feed position and alignment error. These feeds were expected nearly 50% efficiency for Gala-V high band(9.6-10.2GHz and 12.8-14.4GHz). Lower frequency is defined by cut-off of the waveguide, it is clearly shown in figures. The efficiency gradually downs to higher frequency and cross 30% at 15GHz, so 15GHz is concluded as practical upper limit. This degradation is not so severe problem, thus may be fixed in next replacement or maintenance time.

4. Plans

Complete IGUANA feed is delayed due to production schedule of its complexed waveguides. However, we can use 6.5-15GHz with the prototype daughter feed in 34m antenna.

The new feed will replace previous wideband feed of MARBLE and bring better efficiency. Another new feed will be used in 34m for Gala-V before the production of IGUANA completes.

All of our wideband feeds now are used in single linear polarization with commercial waveguide-SMA converter. Dual polarization output will be designed in 2014 for replacement of single-pol output.

Acknowledgement:

Extension of receiver band for methanol masers of this work was achieved with the grant of Joint Development Research supported by the Research Coordination Committee, National Astronomical Observatory of Japan (NAOJ).

The new feed was developed with the incentive fund in NICT in FY2013.

Also, all of our wideband feeds were made in the Workshop of NICT.

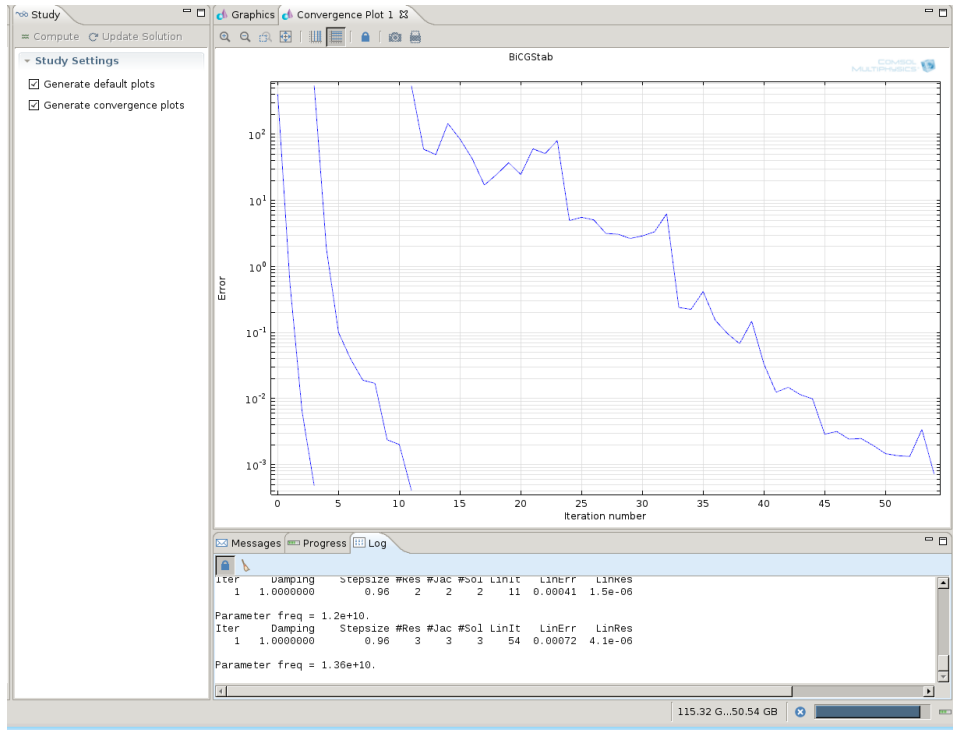


Figure 5. An example of convergence time in COMSOL. the solution time for 12GHz is 10th longer than 8GHz.

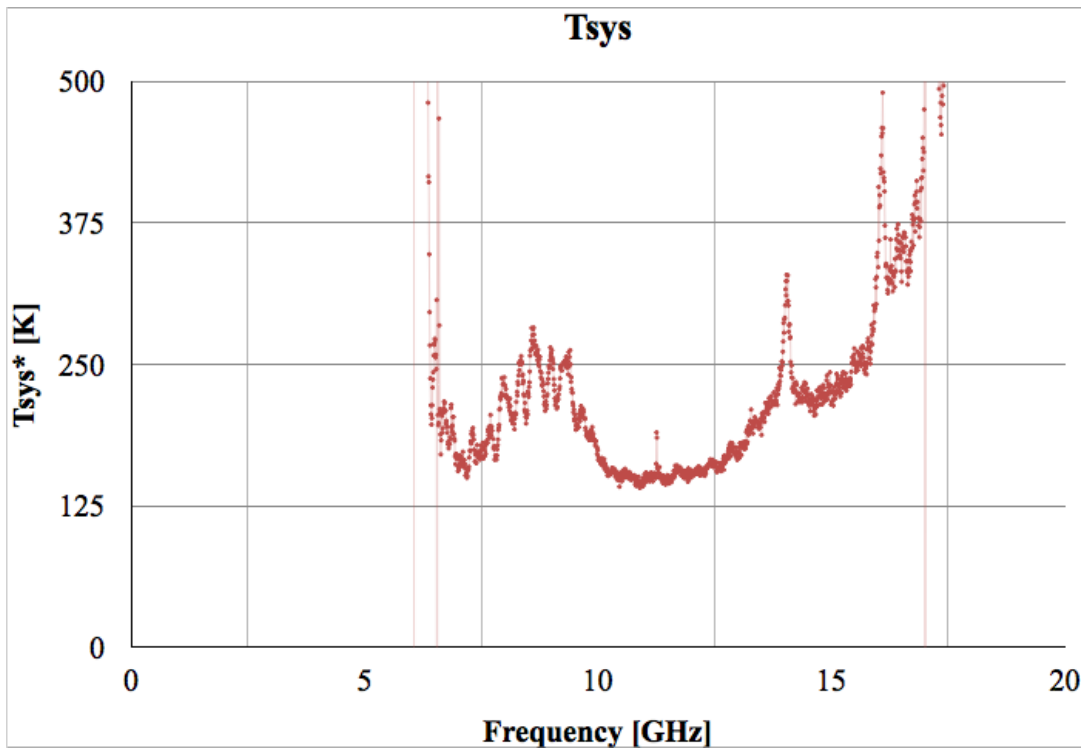


Figure 6. T_{sys} of 34m with No.2 test feed

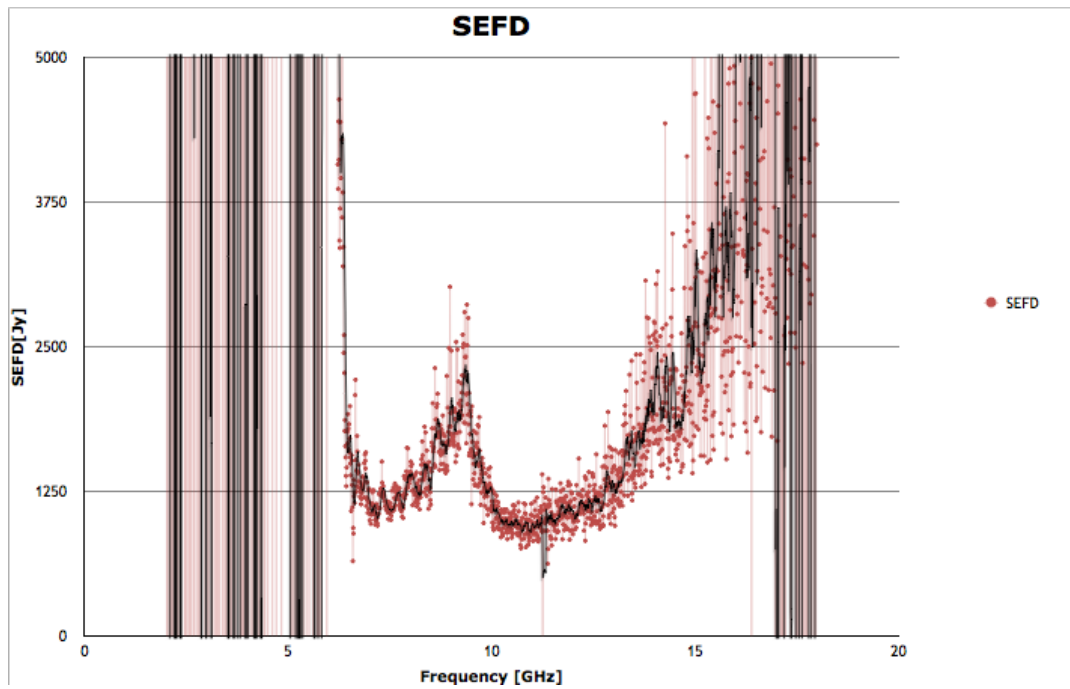


Figure 7. SEFD of 34m with No.2 prototype feed. Solid line shows moving average of 10 points

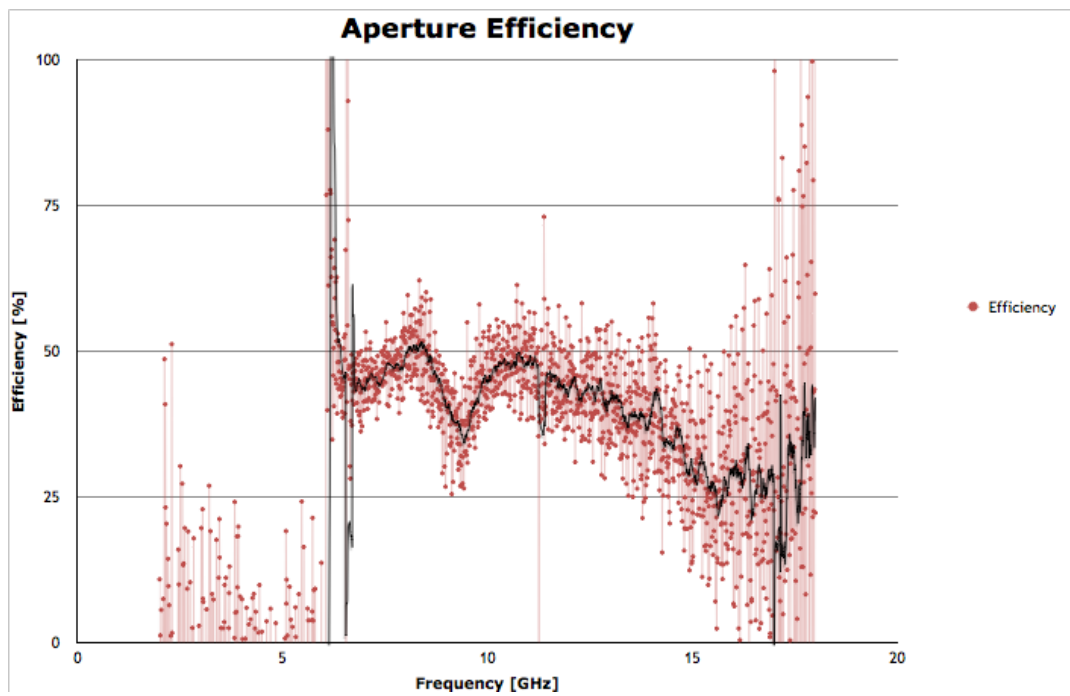


Figure 8. Aperture efficiency of 34m with No.2 prototype feed. Solid line shows moving average of 10 points

~ News ~

The 13th IVS NICT- Technology Development Center Symposium

The 13th VLBI Technology Development Center Symposium was held on June 4th in 2014 at the Kashima Space Technology Center. This symposium has been held annually since 2001. At the end of this March 2014, three big leaders of Japanese VLBI community have formally retired. They are Prof. Fujinobu Takahashi of Yokohama National University, Prof. Noriyuki Kawaguchi of National Astronomical Observatory of Japan(NAOJ), and Dr. Tetsuro Kondo of NICT. They started VLBI carrier from Radio Research Laboratory (current NICT) and played great leadership in especially technology development in VLBI community. This symposium was held with meaning of memorizing their achievements, too.

Seventeen talks were presented in the symposium, which include variety of VLBI research subjects from technology developments to scientific observations. Although proceeding papers of following presentations are not included in this issue, they suggest fruitful aspects of further VLBI technology developments: “Improvements of Delta-DOR measurements for Spacecraft Navigation” by Dr. Takeuchi of JAXA/ISAS, two talks on “Development of balloon VLBI observation system for higher frequency VLBI” by Dr. Okada of Osaka Prefecture Univ. and by Dr. Kono of NAOJ., “Big data of space geodesy achieved by the database system and log records management” by Prof. Takahashi of Yokohama National Univ., “Study on synchrotron emission mechanism from Jupiter” by Dr. Kita of Tohoku Univ., “VLBI observation with Internet and Opt-link” by Prof. Takaba of Gifu Univ., and “Current status of Ibaraki VLBI station (Hitachi and Takahagi)” by Dr. Yonekura of Ibaraki Univ.

We thank all the contributions to this symposium and to proceeding papers of this issue.

On behalf of VLBI group of NICT.
Space and Time Standards Laboratory
Mamoru Sekido



Figure 1. Group Photo of the participants of the 13th IVS NICT-TDC Symposium on 4th June 2014.

“IVS NICT Technology Development Center News” (IVS NICT-TDC News) published by the National Institute of Information and Communications Technology (NICT) (former the Communications Research Laboratory (CRL)) is the continuation of “IVS CRL Technology Development Center News” (IVS CRL-TDC News). (On April 1, 2004, Communications Research Laboratory (CRL) and Telecommunications Advancement Organization of JAPAN (TAO) were reorganized as “National Institute of Information and Communications Technology (NICT)”.)

VLBI Technology Development Center (TDC) at NICT is supposed

- 1) to develop new observation techniques and new systems for advanced Earth’s rotation observations by VLBI and other space techniques,
- 2) to promote research in Earth rotation using VLBI,
- 3) to distribute new VLBI technology,
- 4) to contribute the standardization of VLBI interface, and
- 5) to deploy the real-time VLBI technique.

The NICT TDC newsletter (IVS NICT-TDC News) is published biannually by NICT.

This news was edited by Mamoru SEKIDO, Kashima Space Technology Center. Inquires on this issue should be addressed to Mamoru SEKIDO, Kashima Space Technology Center, National Institute of Information and Communications Technology, 893-1 Hirai, Kashima, Ibaraki 314-8501, Japan, e-mail : sekido@nict.go.jp.

Summaries of VLBI and related activities at the National Institute of Information and Communications Technology are on the Web. The URL to view the home page of the Radio Astronomy Applications Section of the Space-Time Measurement Group of Space-Time Standards Laboratory is : “http://www2.nict.go.jp/aeri/sts/stmg/index_e.html”.

IVS NICT TECHNOLOGY DEVELOPMENT CENTER NEWS No.34, October 2014

International VLBI Service for Geodesy and Astrometry

NICT Technology Development Center News

published by

National Institute of Information and Communications Technology, 4-2-1 Nukui-kita, Koganei,
Tokyo 184-8795, Japan

